Available online at www.sciencedirect.com

ScienceDirect

Journal of the Franklin Institute 352 (2015) 5569–5598

Journal of The Franklin Institute

www.elsevier.com/locate/jfranklin

Vision-based navigation and guidance of a sensorless missile ☆

S.S. Mehta[a,*], C. Ton[b], Z. Kan[c], J.W. Curtis[d]

[a]Department of Industrial and Systems Engineering, University of Florida, Research and Engineering Education Facility, Shalimar, FL 32579, USA

[b]National Research Council, Air Force Research Laboratory, Eglin AFB, FL 32542, USA

[c]Department of Mechanical and Aerospace Engineering, University of Florida, Research and Engineering Education Facility, Shalimar, FL 32579, USA

[d]Air Force Research Laboratory, Munitions Directorate, Eglin AFB, FL 32542, USA

Received 13 March 2015; accepted 13 September 2015
Available online 9 October 2015

Abstract

The objective of this paper is to develop a vision-based terminal guidance system for sensorless missiles. Specifically, monocular vision-based relative navigation and robust control methods are developed for a sensorless missile to intercept a ground target maneuvering with unknown time-varying velocity. A mobile wireless sensor and actor network is considered wherein a moving airborne monocular camera (e.g., attached to an aircraft) provides image measurements of the missile (actor) while another moving monocular camera (e.g., attached to a small UAV) tracks a ground target. The challenge is to express the unknown time-varying target position in the time-varying missile frame using image feedback from cameras moving with unknown trajectories. In a novel relative navigation approach, assuming the knowledge of a single geometric length on the missile, the time-varying target position is obtained by fusing the daisy-chained image measurements of the missile and the target into a homography-based Euclidean reconstruction method. The three-dimensional interception problem is posed in pursuit guidance, proportional navigation, and the proposed hybrid guidance framework. Interestingly, it will be shown that by appropriately defining the error system a single control structure can be maintained across all the above guidance methods. The control problem is formulated in terms of target dynamics in a 'virtual' camera mounted on the missile, which enables design of an adaptive nonlinear visual servo controller that compensates for the unknown

☆This research is supported in part by a grant from the AFRL Mathematical Modeling and Optimization Institute contracts FA8651-08-D-0108/042,043,049 and the USDA NIFA AFRI National Robotics Initiative 2013-67021-21074. Any opinions, findings and conclusions or recommendations expressed in this material are those of the author(s) and do not necessarily reflect the views of the funding agency.

*Corresponding author. Tel.: +1 850 833 9350; fax: +1 850 833 9366.
E-mail address: siddhart@ufl.edu (S.S. Mehta).

http://dx.doi.org/10.1016/j.jfranklin.2015.09.010

time-varying missile–target relative velocity. Stability and zero-miss distance analysis of the proposed controller is presented, and a high-fidelity numerical simulation verifies the performance of the guidance laws.

1. Introduction

Homing guidance and remote control guidance are typically used in the control of a missile to intercept a maneuvering target. Missiles employing homing guidance can detect a target using an on-board seeker, and subsequently guide itself to intercept the target. The on-board sensors (e.g., radar and camera) and a guidance computer along with the corresponding additional power requirement can result in higher cost and larger missile footprint. Besides the naive motivation to reduce the unit cost, it is also notable that the modern military aircrafts with internal weapons bays for advanced stealth capability impose a restriction on the size of the ballistics. In the view of cost and size constraints, it may be beneficial to consider remote control guidance systems. In contrast to homing guidance, the sensor payload in remote control guidance can be located off-board the missile, and the control commands are transmitted to the missile over a communication channel. Thus, enabling a low cost, small footprint missile design with only a communication link to the guidance computer. However, the existing remote control guidance methods have several limitations as follows. Remote control guidance relies on active sensors (e.g., radar and laser) to illuminate and identify the location of the target which can provide an early warning to the target. It is also well known that pure command guidance has inaccuracies during the terminal phase due to excess glint noise, cf. Miwa et al. [20], Nesline and Zarchan [21], and Uhrmeister [29], and the lack of resolution as the distance of the target from the sensor becomes large. Retransmission homing, or track-via-missile, system overcomes this drawback by employing a radar receiver on the missile to locate target during the terminal phase. Nevertheless, the missile relies on a ground-based radar to illuminate target, therefore it will be unable to engage the target if it moves out of the radar's envelop, or it is hidden by an obstacle. Also, the radar system itself can be at risk from anti-radiation missiles and radar jammers [25]. As a result, the motivation behind the presented work is to develop a remote control guidance system using monocular cameras for terminal guidance of a sensorless missile. In spite of the advantages, there has been little research activity that uses vision-only off-board seekers for command guidance. For completeness, relevant and interesting results using monocular vision for homing missile guidance are presented below.

Optical flow based circular navigation guidance (CNG) law for three-dimensional intercepts is presented by Manchester et al. [14], where the optical flow of the target measured in an on-board camera provides the line-of-sight (LOS) angular rate measurements. The CNG law in Manchester et al. [14] is primarily developed to intercept target with an impact angle constraint, and it is proved to perform satisfactorily when the target is stationary, or the velocity of the target is known [15]. Pathirana and Savkin [23] developed a robust extended Kalman filter based sensor fusion method to improve performance of vision-guided homing missiles by combining measurements from an on-board camera with information from a ground radar or other imaging devices, for example, cameras mounted on unmanned aerial vehicles (UAVs). In Pathirana and Savkin [23], a standard augmented proportional navigation guidance (APNG) law was employed

with the obtained target state estimates to achieve interception. The results given in Pathirana and Savkin [23] were extended in Malyavej et al. [13] by including bit rate constraint for communication channels. However, the results in Pathirana and Savkin [23] and Malyavej et al. [13] assume that the absolute position and velocity of the cameras is known. Tian et al. [28] developed an adaptive guidance law to intercept a maneuvering target using an on-board camera by assuming the target acceleration as an unknown time-varying bounded disturbance. The controller in Tian et al. [28] guarantees uniformly ultimately bounded (UUB) stability of the system states. A vision-based integrated guidance controller was presented in Mehta et al. [19] to intercept a stationary or a non-accelerating target in the presence of uncertain missile dynamics. In Mehta et al. [19], a globally asymptotically stable control law was derived for six degrees-of-freedom missile control. Though successful in their respective control endeavors, the previous research mentioned above considers missile guidance with an on-board monocular camera. To the best knowledge of the authors, the problem of employing off-board imaging seekers alone to navigate and control sensorless missiles in GPS-denied environments remains at large unsolved.

The contribution of this work is twofold: First, we propose a novel daisy-chaining based sensing to enable relative navigation of a sensorless missile using off-board vision sensors alone. Second, the well-known pursuit guidance and parallel navigation approaches along with the introduced hybrid guidance are formulated in a unified vision-based control framework to intercept a target maneuvering with unknown velocity. We consider a mobile wireless sensor and actor network (MWSAN) where a moving airborne monocular camera (e.g., attached to an UAV or aircraft) maintains a missile in the field-of-view while another moving monocular camera (e.g., attached to a small UAV) tracks a ground target as shown in Fig. 1. The key idea is to enable relative navigation of a missile with respect to a moving target using off-board imaging seekers, thereby eliminating sensor payload and reducing the size of a missile. The application of UAVs in object tracking is well-studied [30], where numerous robust, optimal, and cooperative

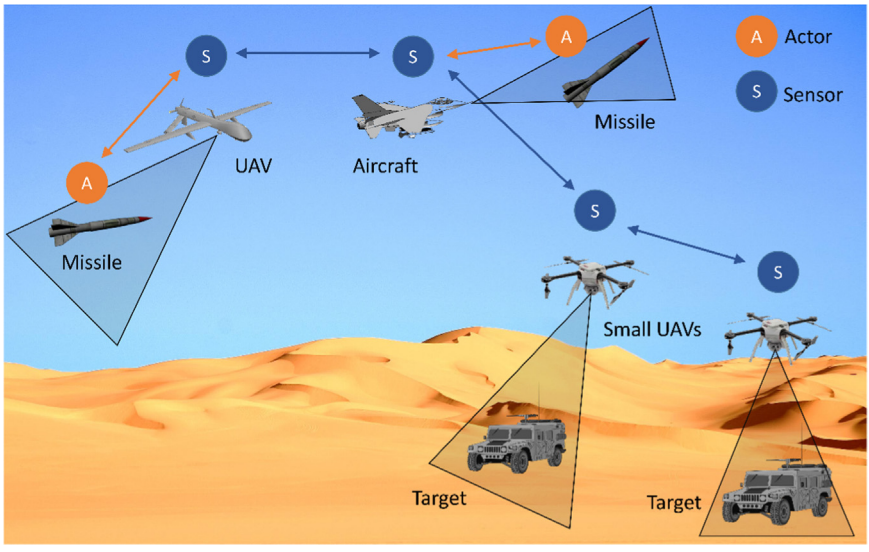

Fig. 1. Problem scenario showing sensors communicating target measurements to actors over a MWSAN.

tracking solutions can be found cf. Stepanyan and Hovakimyan [26], Shaferman and Shima [24], Summers et al. [27], Chen et al. [2], Ergezer and Leblebicioglu [6], Kim et al. [11]. Therefore, it is considered that an UAV or an aircraft traveling at sufficiently high-altitude provides image measurements of a missile during the terminal stage, while a small UAV tracks a maneuvering target close to ground. The imaging seekers are monocular vision cameras, and, as opposed to Pathirana and Savkin [23] and Malyavej et al. [13], the time-varying position and velocity of the cameras (i.e., UAVs or aircrafts) is considered to be unknown, e.g., due to GPS restrictions. The main challenge is to obtain the time-varying position of a maneuvering target in terms of the time-varying missile frame using image feedback from monocular cameras moving with unknown time-varying trajectories. Based on our previous research in cooperative control of multi-agent systems [16,17], a daisy-chaining approach is proposed to determine the geometric relationship between the time-varying missile, target, and camera coordinate frames. It is well-known in computer vision that without the knowledge of the motion (e.g., velocity) or the object model a monocular camera can provide translation only up to a scale, i.e., the Euclidean depth is unknown. To retrieve the magnitude of translation, we assume the knowledge of a single geometric length on the missile (e.g., the length between two arbitrary markers on the longitudinal axis). The developed daisy-chained formulations can then be used in homography-based Euclidean reconstruction to obtain the time-varying target position in the missile coordinate frame.

Given the target position, a nonlinear adaptive controller is presented for a bank-to-turn (BTT)[1] missile to intercept a maneuvering target. To allow distributed control, the guidance computer is considered to be located on the missile, and the target position is communicated by the sensors to the missile over a MWSAN as shown in Fig. 1. The guidance problem is formulated in vision-based framework by assuming a *virtual* camera strapped to the missile, which aids in designing an adaptive controller to compensate for the unknown missile–target relative motion. Apart from posing pursuit guidance [18] and proportional navigation in vision-based framework, we propose a hybrid guidance law that maintains the target at constant LOS in the missile body frame. In vision-based formulation, hybrid guidance becomes an extension of pursuit guidance and retains simplicity but does not exhibit the strong tail-chasing behavior. Further, hybrid guidance only requires the knowledge of the target position – as opposed to proportional navigation which requires an additional orientation measurement of the missile – thereby demanding less communication bandwidth. Interestingly, it will be shown that by appropriately selecting the error system, a single control structure can be maintained across all the three guidance laws. The developed image-based visual servo (IBVS) control problem has several advantages, including reduced computation time, robustness to inaccuracies in camera calibration [34], and the ability to maintain the target in the field-of-view via feature-based motion strategies [3]. To address the issue of robustness with respect to exogenous disturbances (e.g., wind gusts), a continuous, robust feedback element is included in the guidance law, which compensates for the unknown, bounded, nonlinear disturbances. High-fidelity numerical simulation verifies the performance of the proposed relative navigation and guidance laws under various target maneuvers.

[1]The linear velocity of a missile is produced by means of a propulsion system, where the thrust force is uncontrolled and directed along the missile longitudinal axis [31]; it is assumed that the missile linear velocity is unknown and unmeasurable. For the BTT type of missile systems, the heading change is obtained by aerodynamic control surface deflections for pitch, yaw, and roll angles. Therefore, the control objective is to design angular rate commands in roll, pitch, and yaw directions to intercept a target.

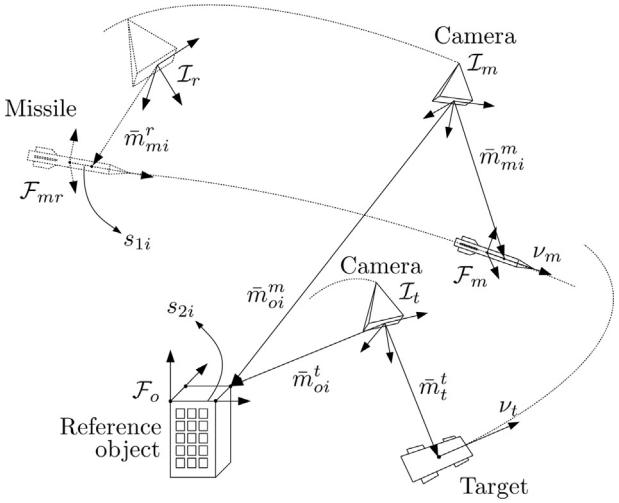

Fig. 2. Coordinate frame relationship between the missile, cameras, target, and reference object.

2. Geometric model

Consider a monocular camera with an attached time-varying coordinate frame $\mathcal{I}_m$ that is navigating (e.g., by remote controlled aircraft) above a missile during terminal stage as depicted in Fig. 2. Consider the time-varying coordinate frame $\mathcal{F}_m$ whose origin is attached to the center of gravity of the missile airframe, a body-carried coordinate frame $\mathcal{F}_r$ with the origin at the missile center of gravity and orientation fixed to a north-east-down (NED) navigation frame, and an Earth-fixed reference system (ESF) $\mathcal{F}_e$ on the surface of Earth. Compared to the range of a vision-guided missile, it can be assumed that Earth's curvature is negligible; therefore, the orientation of coordinate frame $\mathcal{F}_r$ is considered to coincide with that of frame $\mathcal{F}_e$. The missile is represented in the camera image by four[2] feature points that are coplanar and not collinear. The Euclidean position of the feature points from the origin of $\mathcal{F}_m$ is denoted by $s_{1i} \in \mathbb{R}^3 \ \forall i = 1,2,3,4$. The plane defined by the missile feature points is denoted by π_m. The feature points that define π_m are also assumed to be visible when the camera $\mathcal{I}_m$ is located coincident with the position and orientation (i.e., pose) of the stationary coordinate frame $\mathcal{I}_r$. Without loss of generality, the reference camera pose $\mathcal{I}_r$ is considered to be the initial (i.e., at time $t=0$) pose of the camera frame $\mathcal{I}_m$. Also, let $\mathcal{F}_{mr}$ denote the pose of the time-varying missile frame $\mathcal{F}_m$ at $t=0$. The linear and angular velocity of the missile expressed in $\mathcal{F}_m$ with respect to $\mathcal{F}_e$ is denoted by $\nu_m(t) \in \mathbb{R}^3$ and $\omega_m(t) \in \mathbb{R}^3$, respectively.

While viewing the feature points of the missile, the camera $\mathcal{I}_m$ is assumed to view four additional coplanar and noncollinear feature points of a stationary reference object (e.g., a structure on the ground). The four additional feature points define the plane π_o. The stationary coordinate frame $\mathcal{F}_o$ is attached to the object, where $s_{2i} \in \mathbb{R}^3 \ \forall i = 1,2,3,4$ denotes the position

[2]Image analysis methods can be used to determine planar objects (e.g. through color, texture differences). These traditional computer vision methods can be used to help determine and isolate the four coplanar feature points. If four coplanar target points are not available then the subsequent development can exploit the classic eight-points algorithm [12] with no four of the eight target points being coplanar.

Table 1
Rotation and translation vectors between various coordinate frames.

Motion	Coordinate frames
$R_m^m(t)$, $x_{fm}^m(t)$	$\mathcal{I}_m$ to $\mathcal{F}_m$
$R_o^m(t)$, $x_{fo}^m(t)$	$\mathcal{I}_m$ to $\mathcal{F}_o$
R_o^r, x_{fo}^r	$\mathcal{I}_r$ to $\mathcal{F}_o$
R_m^r, x_{fm}^r	$\mathcal{I}_r$ to $\mathcal{F}_{mr}$
$R_o^t(t)$, $x_{fo}^t(t)$	$\mathcal{I}_t$ to $\mathcal{F}_o$
$R_t^m(t)$, $x_{ft}^m(t)$	$\mathcal{I}_m$ to $\mathcal{I}_t$
$R_m^t(t)$, $x_{fm}^t(t)$	$\mathcal{I}_t$ to $\mathcal{I}_m$

of the feature points from the origin of $\mathcal{F}_o$. It is to be noted that no assumption has been made regarding the motion of the camera $\mathcal{I}_m$ with respect to planes π_o and π_m.

Another monocular camera with an attached time-varying coordinate frame $\mathcal{I}_t$ is dedicated to track a ground target as shown in Fig. 2. The point mass target is represented in the camera image by a single feature point thereby reducing image processing burden. The target is assumed to maneuver on the ground with an unknown time-varying velocity $v_t(t) \in \mathbb{R}^3$ with respect to $\mathcal{F}_e$. The camera $\mathcal{I}_t$ is also assumed to observe the feature points of the stationary reference object $\mathcal{F}_o$. Similar to frame $\mathcal{I}_m$, no assumption is made regarding the motion of $\mathcal{I}_t$ with respect to plane π_o. Table 1 shows the relationships between various coordinate frames.

Assumption 1. The distance $\|s_{1i}\|$ and $\|s_{2i}\|$ from the origin of $\mathcal{F}_m$ and $\mathcal{F}_o$, respectively, to one of the feature points on π_m and π_o, respectively, is assumed to be known, i.e., a single geometric length on the missile and the reference object is available.

To relate the coordinate systems, let $R_m^m(t)$, $R_o^m(t)$, R_o^r, R_m^r, $R_o^t(t)$, $R_t^m(t)$, $R_m^t(t) \in \mathbb{SO}(3)$ denote the rotation from $\mathcal{I}_m$ to $\mathcal{F}_m$, $\mathcal{I}_m$ to $\mathcal{F}_o$, $\mathcal{I}_r$ to $\mathcal{F}_o$, $\mathcal{I}_r$ to $\mathcal{F}_{mr}$, $\mathcal{I}_t$ to $\mathcal{F}_o$, $\mathcal{I}_m$ to $\mathcal{I}_t$, and $\mathcal{I}_t$ to $\mathcal{I}_m$, respectively, $x_{fm}^m(t)$, $x_{fo}^m(t)$, $x_{ft}^m(t) \in \mathbb{R}^3$ denote the respective time-varying translation from $\mathcal{I}_m$ to $\mathcal{F}_m$, $\mathcal{I}_m$ to $\mathcal{F}_o$, and $\mathcal{I}_m$ to $\mathcal{I}_t$ with coordinates expressed in $\mathcal{I}_m$, $x_{fo}^r, x_{fm}^r \in \mathbb{R}^3$ denote the constant translation from $\mathcal{I}_r$ to $\mathcal{F}_o$ and $\mathcal{I}_r$ to $\mathcal{F}_{mr}$, respectively, expressed in $\mathcal{I}_r$, and $x_{fo}^t(t)$, $x_{fm}^t(t) \in \mathbb{R}^3$ denote the respective time-varying translation from $\mathcal{I}_t$ to $\mathcal{F}_o$ and $\mathcal{I}_t$ to $\mathcal{I}_m$ expressed in the coordinates of $\mathcal{I}_t$. From the geometry between the coordinate frames depicted in Fig. 2, the following relationships can be developed:

$$\overline{m}_{mi}^m = x_{fm}^m + R_m^m s_{1i}, \quad \overline{m}_{oi}^m = x_{fo}^m + R_o^m s_{2i} \tag{1}$$

$$\overline{m}_{mi}^r = x_{fm}^r + R_m^r s_{1i}, \quad \overline{m}_{oi}^r = x_{fo}^r + R_o^r s_{2i} \tag{2}$$

$$\overline{m}_{oi}^t = x_{fo}^t + R_o^t s_{2i} \tag{3}$$

where $\overline{m}_{mi}^m(t)$, $\overline{m}_{oi}^m(t) \in \mathbb{R}^3$ denote the time-varying Euclidean coordinates of the feature points of the missile and reference object, respectively, expressed in $\mathcal{I}_m$ as

$$\overline{m}_{mi}^m(t) \triangleq \left[x_{mi}^m(t) \;\; y_{mi}^m(t) \;\; z_{mi}^m(t)\right]^T \tag{4}$$

$$\overline{m}_{oi}^m(t) \triangleq \left[x_{oi}^m(t) \;\; y_{oi}^m(t) \;\; z_{oi}^m(t)\right]^T, \tag{5}$$

$\overline{m}^r_{mi}, \overline{m}^r_{oi} \in \mathbb{R}^3$ denotes the constant Euclidean coordinates of the feature points of the missile at $\mathcal{F}_{mr}$ and the reference object, respectively, expressed in $\mathcal{I}_r$ as

$$\overline{m}^r_{mi} \triangleq \left[x^r_{mi} \;\; y^r_{mi} \;\; z^r_{mi}\right]^T \tag{6}$$

and $\overline{m}^t_{oi}(t) \in \mathbb{R}^3$ denotes the time-varying Euclidean coordinates of the feature points of the reference object expressed in $\mathcal{I}_t$ as

$$\overline{m}^t_{oi}(t) \triangleq \left[x^t_{oi}(t) \;\; y^t_{oi}(t) \;\; z^t_{oi}(t)\right]^T. \tag{7}$$

After algebraic manipulation, the expressions for $\overline{m}^m_{mi}(t)$, $\overline{m}^m_{oi}(t)$, $\overline{m}^r_{mi}$, $\overline{m}^r_{oi}$, and $\overline{m}^t_{oi}(t)$ in Eqs. (1)–(3) can be rewritten as

$$\overline{m}^r_{mi} = \overline{x}^r_{fm} + \overline{R}^r_m \overline{m}^m_{mi} \tag{8}$$

$$\overline{m}^r_{oi} = \overline{x}^r_{fo} + \overline{R}^r_o \overline{m}^m_{oi} \tag{9}$$

$$\overline{m}^m_{oi} = x^m_{ft} + R^m_t \overline{m}^t_{oi} \tag{10}$$

$$\overline{m}^t_{oi} = x^t_{fm} + R^t_m \overline{m}^m_{oi} \tag{11}$$

where $\overline{R}^r_m(t)$, $\overline{R}^r_o(t)$, $R^m_t(t)$, $R^t_m(t) \in \mathbb{SO}(3)$ and $\overline{x}^r_{fm}(t)$, $\overline{x}^r_{fo}(t)$, $x^m_{ft}(t)$, $x^t_{fm}(t) \in \mathbb{R}^3$ are new rotational and translational variables respectively defined as

$$\overline{R}^r_m = R^r_m R^{mT}_m, \quad \overline{R}^r_o = R^r_o R^{mT}_o \tag{12}$$

$$R^m_t = R^m_o R^{t\,T}_o, \quad R^t_m = R^t_o R^{mT}_o \tag{13}$$

$$\overline{x}^r_{fm} = x^r_{fm} - R^r_m R^{mT}_m x^m_{fm} \tag{14}$$

$$\overline{x}^r_{fo} = x^r_{fo} - R^r_o R^{mT}_o x^m_{fo} \tag{15}$$

$$x^m_{ft} = x^m_{fo} - R^m_o R^{t\,T}_o x^t_{fo} \tag{16}$$

$$x^t_{fm} = x^t_{fo} - R^t_o R^{mT}_o x^m_{fo}. \tag{17}$$

Remark 1. Since both the camera and the missile are moving with respect to an inertial frame of reference, the rotation $\overline{R}^r_m(t)$ and translation $\overline{x}^r_{fm}(t)$ in Eqs. (12) and (14), respectively, represent the relative motion of the missile between frames $\mathcal{F}_{mr}$ and $\mathcal{F}_m$ expressed in time-varying frame $\mathcal{I}_m$. However, it will be clear from the subsequent development that the expression in Eq. (8) is sufficient to relate $\mathcal{F}_m$ to $\mathcal{I}_m$ given a single geometric length $\|s_{1i}\|$ on the missile.

By using the projective relationships (see Fig. 2)

$$d^m_m = n^{mT}_m \overline{m}^m_{mi}, \quad d^m_o = n^{mT}_o \overline{m}^m_{oi} \tag{18}$$

$$d^t_o = n^{t\,T}_o \overline{m}^t_{oi} = n^{t\,T}_o \overline{m}^t_t \tag{19}$$

the relationships in Eqs. (8)–(11) can be expressed as

$$\overline{m}^r_{mi} = \left(\overline{R}^r_m + \frac{\overline{x}^r_{fm}}{d^m_m} n^{mT}_m\right) \overline{m}^m_{mi} \tag{20}$$

$$\overline{m}_{oi}^{r} = \left(\overline{R}_{o}^{r} + \frac{\overline{x}_{fo}^{r}}{d_{o}^{m}} n_{o}^{m\,T}\right)\overline{m}_{oi}^{m} \tag{21}$$

$$\overline{m}_{oi}^{m} = \left(R_{t}^{m} + \frac{x_{fi}^{m}}{d_{o}^{t}} n_{o}^{t\,T}\right)\overline{m}_{oi}^{t} \tag{22}$$

$$\overline{m}_{oi}^{t} = \left(R_{m}^{t} + \frac{x_{fm}^{t}}{d_{o}^{m}} n_{o}^{m\,T}\right)\overline{m}_{oi}^{m}. \tag{23}$$

In Eqs. (18)–(23), $d_{m}^{m}(t)$, $d_{o}^{t}(t)$, $d_{o}^{m}(t) > \varepsilon$ for $\varepsilon \in \mathbb{R}^{+}$, $n_{m}^{m}(t)$, $n_{o}^{m}(t) \in \mathbb{R}^{3}$ denote the time-varying unit normal from $\mathcal{I}_{m}$ to the planes π_{m} and π_{o}, respectively, and $n_{o}^{t}(t) \in \mathbb{R}^{3}$ denotes the time-varying unit normal from $\mathcal{I}_{t}$ to the plane π_{o}. In Eq. (19), $\overline{m}_{t}^{t}(t) \in \mathbb{R}^{3}$ denotes the unknown time-varying Euclidean coordinates of the target expressed in the time-varying camera frame $\mathcal{I}_{t}$.

3. Relative navigation

The relationships given by Eqs. (20)–(23) provide a means to quantify rotation and translation between the different coordinate frames. In the absence of model or motion knowledge, a monocular vision system can only yield translation scaled by an unknown scaling factor. To enable relative navigation, the translation scaling factor along with the Euclidean position and orientation of various coordinate frames should be recovered.

A homography-based relative navigation approach is presented by fusing the daisy-chained relationships in Eqs. (20)–(23) with a geometric reconstruction method to determine the time-varying position of the target with respect to the missile frame $\mathcal{F}_{m}$. The expressions of Euclidean homographies between $\mathcal{I}_{r}$ and $\mathcal{I}_{m}$ and $\mathcal{I}_{m}$ and $\mathcal{I}_{t}$ can be obtained. Subsequently, the projective homography relationships can be evaluated to relate the different coordinate frames. Using a known geometric length on the missile and the reference object (Assumption 1), the geometric reconstruction method in Gans et al. [9] can be used to determine the unknown translation scaling factors along with the time-varying position of the target.

To facilitate the subsequent development, the normalized Euclidean coordinates of the feature points on the missile and the reference object, denoted by $m_{mi}^{m}(t)$, $m_{oi}^{m}(t) \in \mathbb{R}^{3}$, respectively, can be expressed in terms of $\mathcal{I}_{m}$ as

$$m_{mi}^{m} \triangleq \frac{\overline{m}_{mi}^{m}}{z_{mi}^{m}}, \quad m_{oi}^{m} \triangleq \frac{\overline{m}_{oi}^{m}}{z_{oi}^{m}} \tag{24}$$

and the normalized Euclidean coordinates of the feature points on the reference object and the target, denoted by $m_{oi}^{t}(t)$, $m_{t}^{t}(t) \in \mathbb{R}^{3}$, respectively, can be expressed in terms of $\mathcal{I}_{t}$ as

$$m_{oi}^{t} \triangleq \frac{\overline{m}_{oi}^{t}}{z_{oi}^{t}}, \quad m_{t}^{t} \triangleq \frac{\overline{m}_{t}^{t}}{z_{t}^{t}}. \tag{25}$$

Similarly, the normalized Euclidean coordinates of the feature points on the missile and the reference object, denoted by $m_{mi}^{r}, m_{oi}^{r} \in \mathbb{R}^{3}$, respectively, can be expressed in terms of $\mathcal{I}_{r}$ as follows:

$$m_{mi}^{r} \triangleq \frac{\overline{m}_{mi}^{r}}{z_{mi}^{r}}, \quad m_{oi}^{r} \triangleq \frac{\overline{m}_{oi}^{r}}{z_{oi}^{r}}. \tag{26}$$

From the expressions given in Eqs. (20), (24) and (26), the rotation and translation between $\mathcal{F}_{mr}$

and $\mathcal{F}_m$ can be related in terms of the normalized Euclidean coordinates as

$$m_{mi}^r = \underbrace{\left(\frac{z_{mi}^m}{z_{mi}^r}\right)}_{\alpha_{mi}} \underbrace{\left(\overline{R}_m^r + \overline{x}_{hm}^r n_m^{mT}\right)}_{H_m} m_{mi}^m. \tag{27}$$

In a similar manner, Eqs. (21), (24) and (26) can be used to relate the rotation and translation between camera frames $\mathcal{I}_m$ and $\mathcal{I}_r$ as

$$m_{oi}^r = \underbrace{\left(\frac{z_{oi}^m}{z_{oi}^r}\right)}_{\alpha_{oi}} \underbrace{\left(\overline{R}_o^r + \overline{x}_{ho}^r n_o^{mT}\right)}_{H_o} m_{oi}^m \tag{28}$$

and Eqs. (22)–(25) can be used to relate the rotation and translation between camera frames $\mathcal{I}_m$ and $\mathcal{I}_t$ as

$$m_{oi}^m = \underbrace{\left(\frac{z_{oi}^t}{z_{oi}^m}\right)}_{\alpha_{oi}^m} \underbrace{\left(R_t^m + x_{ht}^m n_o^{t\,T}\right)}_{H_o^m} m_{oi}^t \tag{29}$$

$$m_{oi}^t = \underbrace{\left(\frac{z_{oi}^m}{z_{oi}^t}\right)}_{\alpha_{oi}^t} \underbrace{\left(R_m^t + x_{hm}^t n_o^{mT}\right)}_{H_o^t} m_{oi}^m. \tag{30}$$

In Eqs. (27)–(30), $\alpha_{mi}(t)$, $\alpha_{oi}(t)$, $\alpha_{oi}^m(t)$, $\alpha_{oi}^t(t) \in \mathbb{R}$ denote time-varying depth ratios, $H_m(t)$, $H_o(t)$, $H_o^m(t)$, $H_o^t(t) \in \mathbb{R}^{3\times 3}$ denote Euclidean homographies [7], and $\overline{x}_{hm}^r(t)$, $\overline{x}_{ho}^r$, $x_{ht}^m(t)$, $x_{hm}^t(t) \in \mathbb{R}^3$ denote scaled translation vectors defined as

$$\overline{x}_{hm}^r \triangleq \frac{\overline{x}_{fm}^r}{d_m^m}, \quad \overline{x}_{ho}^r \triangleq \frac{\overline{x}_{fo}^r}{d_o^m} \tag{31}$$

$$x_{ht}^m \triangleq \frac{x_{ft}^m}{d_o^t}, \quad x_{hm}^t \triangleq \frac{x_{fm}^t}{d_o^m}. \tag{32}$$

Each Euclidean feature point on the missile and reference object will have a projected pixel coordinate expressed in $\mathcal{I}_m$ as

$$p_{mi}^m \triangleq \left[u_{mi}^m \;\; v_{mi}^m \;\; 1\right]^T, \quad p_{oi}^m \triangleq \left[u_{oi}^m \;\; v_{oi}^m \;\; 1\right]^T \tag{33}$$

where $p_{mi}^m(t)$, $p_{oi}^m(t) \in \mathbb{R}^3$ represent the time-varying, homogeneous image-space coordinates of the feature points on the missile and reference object, respectively. The time-varying, homogeneous pixel coordinates $p_{oi}^t(t), p_t^t(t) \in \mathbb{R}^3$ of the reference object and the target, respectively, expressed in $\mathcal{I}_t$ are

$$p_{oi}^t \triangleq \left[u_{oi}^t \;\; v_{oi}^t \;\; 1\right]^T, \quad p_t^t \triangleq \left[u_t^t \;\; v_t^t \;\; 1\right]^T. \tag{34}$$

The camera $\mathcal{I}_t$ communicates the observed pixel coordinates $p_{oi}^t(t)$ and $p_t^t(t)$ to the camera $\mathcal{I}_m$ (observing the missile) over the sensor network to determine the Euclidean position of the target. Similarly, the projected constant pixel coordinates $p_{mi}^r, p_{oi}^r \in \mathbb{R}^3$ of the missile and reference object can be expressed in $\mathcal{I}_r$ as

$$p_{mi}^r \triangleq \left[u_{mi}^r \;\; v_{mi}^r \;\; 1\right]^T, \quad p_{oi}^r \triangleq \left[u_{oi}^r \;\; v_{oi}^r \;\; 1\right]^T. \tag{35}$$

In Eqs. (33)–(35), $u_{mi}^{m}(t)$, $v_{mi}^{m}(t)$, $u_{oi}^{m}(t)$, $v_{oi}^{m}(t)$, $u_{oi}^{t}(t)$, $v_{oi}^{t}(t)$, u_{mi}^{r}, v_{mi}^{r}, u_{oi}^{r}, $v_{oi}^{r} \in \mathbb{R}$. To calculate the Euclidean homographies given in Eqs. (27)–(30) from pixel information, the projected pixel coordinates are related to $m_{mi}^{m}(t)$, $m_{oi}^{m}(t)$, m_{mi}^{r}, m_{oi}^{r}, and $m_{oi}^{t}(t)$ by the pin-hole camera model as

$$p_{mi}^{m} = A_m m_{mi}^{m}, \quad p_{oi}^{m} = A_m m_{oi}^{m} \tag{36}$$

$$p_{mi}^{r} = A_m m_{mi}^{r}, \quad p_{oi}^{r} = A_m m_{oi}^{r}, \quad p_{oi}^{t} = A_t m_{oi}^{t} \tag{37}$$

where A_m, $A_t \in \mathbb{R}^{3\times 3}$ are the known, constant, invertible intrinsic camera calibration matrices of $\mathcal{I}_m$ and $\mathcal{I}_t$, respectively. By using Eqs. (27)–(30), (36) and (37), the following relationships can be developed:

$$p_{mi}^{r} = \alpha_{mi} \underbrace{\left(A_m H_m A_m^{-1}\right)}_{G_m} p_{mi}^{m} \tag{38}$$

$$p_{oi}^{r} = \alpha_{oi} \underbrace{\left(A_m H_o A_m^{-1}\right)}_{G_o} p_{oi}^{m} \tag{39}$$

$$p_{oi}^{m} = \alpha_{oi}^{m} \underbrace{\left(A_m H_o^{m} A_t^{-1}\right)}_{G_o^m} p_{oi}^{t} \tag{40}$$

$$p_{oi}^{t} = \alpha_{oi}^{t} \underbrace{\left(A_t H_o^{t} A_m^{-1}\right)}_{G_o^t} p_{oi}^{m} \tag{41}$$

where $G_m(t) = [g_{mij}(t)]$, $G_o(t) = [g_{oij}(t)]$, $G_o^m = [g_{oij}^m(t)]$, $G_o^t = [g_{oij}^t(t)] \in \mathbb{R}^{3\times 3}$ $\forall i,j = 1,2,3$ denote projective homographies. Sets of linear equations can be developed from Eqs. (38) to (41) to determine the projective homographies up to a scale. Various techniques can be used (e.g., see [8,35]) to decompose the Euclidean homographies to obtain $\alpha_{mi}(t)$, $\alpha_{oi}(t)$, $\alpha_{oi}^{m}(t)$, $\alpha_{oi}^{t}(t)$, $\overline{x}_{hm}^{r}(t)$, $\overline{x}_{ho}^{r}(t)$, $x_{ht}^{m}(t)$, $x_{hm}^{t}(t)$, $\overline{R}_{m}^{r}(t)$, $\overline{R}_{o}^{r}(t)$, $R_{t}^{m}(t)$, $R_{m}^{t}(t)$, $n_{m}^{m}(t)$, $n_{o}^{t}(t)$, and $n_{o}^{m}(t)$.

Without loss of generality, it is assumed that the feature point corresponding to $\overline{m}_{m1}^{m}(t)$ on the missile is at the origin of the frame $\mathcal{F}_m$ (i.e., $\| s_{11} \| = 0$), and the distance $\| s_{12} \| \in \mathbb{R}$ between the feature points corresponding to $\overline{m}_{m1}^{m}(t)$ and $\overline{m}_{m2}^{m}(t)$ is known such that $\| s_{12} \| = \| \overline{m}_{m1}^{m} - \overline{m}_{m2}^{m} \|$. The intersection of $\overline{m}_{m2}^{m}(t)$ with the plane parallel to π_m and passing through $m_{m1}^{m}(t)$, denoted by $m_{m2}^{\prime m}(t) \in \mathbb{R}^3$, can be obtained as

$$m_{m2}^{\prime m} = \frac{n_m^{m} T m_{m1}^{m}}{n_m^{m} T m_{m2}^{m}} m_{m2}^{m} \tag{42}$$

such that the distance $\| s_{12}^{\prime} \| \in \mathbb{R}$ between $m_{m1}^{m}(t)$ and $m_{m2}^{\prime m}(t)$ can be obtained as $\| s_{12}^{\prime} \| = \| m_{m1}^{m} - m_{m2}^{\prime m} \|$. Using the property of similar triangles, the relationship can be developed between $\| s_{12} \|$, $\| s_{12}^{\prime} \|$, $m_{m1}^{m}(t)$, $m_{m2}^{\prime m}(t)$, $\overline{m}_{m1}^{m}(t)$, and $\overline{m}_{m2}^{m}(t)$ as

$$\frac{\| s_{12}^{\prime} \|}{\| s_{12} \|} = \frac{\| m_{m1}^{m} \|}{\| \overline{m}_{m1}^{m} \|} = \frac{\| m_{m2}^{\prime m} \|}{\| \overline{m}_{m2}^{m} \|}. \tag{43}$$

From Eq. (43), the Euclidean coordinates $\overline{m}_{m1}(t)$ and $\overline{m}_{m2}(t)$ can be obtained as

$$\overline{m}_{m1}^{m} = \frac{\| \overline{m}_{m1}^{m} \|}{\| m_{m1}^{m} \|} m_{m1}^{m}, \quad \overline{m}_{m2}^{m} = \frac{\| \overline{m}_{m2}^{m} \|}{\| m_{m2}^{m} \|} m_{m2}^{m}. \tag{44}$$

Since the feature point corresponding to $\overline{m}_{m1}^{m}(t)$ is at the origin of $\mathcal{F}_m$, i.e., $s_{11} = [0\ 0\ 0]^T$, using Eq. (1) the translation $x_{fm}^{m}(t)$ between $\mathcal{F}_m$ and $\mathcal{I}_m$ can be evaluated as $x_{fm}^{m} = \overline{m}_{m1}^{m}$. Using Eq. (44)

and $n_m^m(t)$ from Eq. (38), the rotation R_m^m between $\mathcal{F}_m$ and $\mathcal{I}_m$ can be expressed in terms of orthonormal vectors $i_x, i_y, i_z \in \mathbb{R}^3$ as

$$R_m^m = \begin{bmatrix} i_x & i_y & i_z \end{bmatrix} \begin{cases} i_x = (\overline{m}_{m2}^m - \overline{m}_{m1}^m)/\| s_{12} \| \\ i_y = -n_m^m \times i_x \\ i_z = -n_m^m. \end{cases} \tag{45}$$

In a similar manner, by assuming the feature point corresponding to $\overline{m}_{o1}^m(t)$ on the reference object to be at the origin of $\mathcal{F}_o$ and using the knowledge of the distance $\| s_{22} \| \in \mathbb{R}$, the Euclidean coordinates $\overline{m}_{o1}^m(t)$, $\overline{m}_{o1}^t(t)$, $\overline{m}_{o2}^m(t)$, and $\overline{m}_{o2}^t(t)$ can be obtained along with the rotation matrix $R_o^m(t)$. Using Eqs. (19), (25) and the obtained Euclidean coordinates $\overline{m}_{o1}^t(t)$, the time-varying position $\overline{m}_t^t(t)$ of the target expressed in $\mathcal{I}_t$ can be determined as

$$\overline{m}_t^t = \left(\frac{d_o^t}{n_o^{t\,T} m_t^t} \right) m_t^t = \left(\frac{n_o^{t\,T} \overline{m}_{o1}^t}{n_o^{t\,T} m_t^t} \right) m_t^t. \tag{46}$$

From the geometry between $\mathcal{I}_t$ and $\mathcal{I}_m$ and using Eq. (46) along with the obtained Euclidean coordinates $\overline{m}_{o1}^t(t)$ and $\overline{m}_t^t(t)$, the Euclidean position of the target in $\mathcal{I}_m$, denoted by $\overline{m}_t^m(t) \in \mathbb{R}^3$, can be obtained as

$$\overline{m}_t^m = R_m^{t\,T} \left(\overline{m}_t^t - \overline{m}_{o1}^t + R_m^t \overline{m}_{o1}^m \right). \tag{47}$$

The target position obtained in Eq. (47) can be expressed in terms of the missile coordinate frame $\mathcal{F}_m$, denoted by $\overline{m}_t(t) = \left[x_t(t)\ y_t(t)\ z_t(t) \right]^T$, as

$$\overline{m}_t = R_m^{mT} \left(\overline{m}_t^m - x_{fm}^m \right) \tag{48}$$

where the coordinate frame relationships between $\mathcal{F}_m$ and $\mathcal{I}_m$ given by $x_{fm}^m = \overline{m}_{m1}^m$ and Eq. (45) are used.

Without loss of generality, let $\mathcal{F}_o$ attached to the reference object be the ESF frame $\mathcal{F}_e$. Therefore, the body-carried coordinate frame $\mathcal{F}_r$ will have the orientation as that of $\mathcal{F}_o$. The target position in $\mathcal{F}_r$, denoted by $\overline{m}_t'(t) = \left[x_t'(t)\ y_t'(t)\ z_t'(t) \right]^T$, can be obtained as

$$\overline{m}_t' = R_o^{mT} R_m^m \overline{m}_t. \tag{49}$$

By fusing the daisy-chained Euclidean relationships with the geometric reconstruction method, we have identified the time-varying position of the target expressed in the time-varying missile coordinate frame using image feedback from the monocular cameras $\mathcal{I}_m$ and $\mathcal{I}_t$. The time-varying target position, $\overline{m}_t(t)$ or $\overline{m}_t'(t)$ depending on the guidance method employed, is communicated to the missile $\mathcal{I}_m$ over the network channel. The next objective is to design a controller to intercept the target.

4. Target image dynamics

Consider a *virtual* camera mounted at the origin of $\mathcal{F}_m$. The target dynamics are expressed in terms of the virtual camera as the approach facilitates to compensate for the unknown missile–target relative motion. In addition, it also enables us to maintain a single control structure across pursuit guidance, proportional navigation, and hybrid guidance. Let $\mathcal{I}_v$ denote the body-fixed rotating coordinate frame, coincident with $\mathcal{F}_m$, attached to the virtual camera. The normalized Euclidean coordinates, $m_t(t) \in \mathbb{R}^3$, of the target can be expressed in $\mathcal{I}_v$ as $m_t \triangleq \overline{m}_t / z_t$.

Remark 2. The target is assumed to be in front of the camera, i.e., $z_t(t) > \varepsilon$, where $\varepsilon \in \mathbb{R}^+$. However, the impact happens for some set $z_t \in [z_{\min}, z_{\max}]$, where $z_{\max} \geq z_{\min} > 0$ [10,32]. This is due to the fact that the exact intercept value (i.e., the "zero intercept") depends on the size of the ballistic target and the relative position of the camera at impact.

The pin-hole camera model can be used to determine the virtual pixel coordinates $p_t(t) = [u_t(t)\ v_t(t)]^T \in \mathbb{R}^2$ of the target in the image plane as $u_t = fax_t/z_t + u_o$ and $v_t = fby_t/z_t + v_o$, where f, a, $b \in \mathbb{R}$ are user-defined, constant focal length and scaling factors along the image axes of the virtual camera $\mathcal{I}_v$; $p_o = [u_o\ v_o]^T \in \mathbb{R}^2$ denote the constant coordinates of the principal point (i.e., the intersection of an optical axis with the image plane) of the camera. Taking the time derivative of $p_t(t)$, the velocity of the missile and the target can be related to the velocity $\dot{p}_t(t) \in \mathbb{R}^2$ of the feature point in the image plane as

$$\dot{p}_t = \frac{J_\nu}{z_t}\left(\nu_m - \nu_t^m\right) + J_\omega \omega_m + d \tag{50}$$

where $\nu_m(t) \in \mathbb{R}^3$ is the unknown time-varying linear velocity of the missile, $\nu_t^m(t) \in \mathbb{R}^3$ is the unknown time-varying velocity of the target expressed in $\mathcal{F}_m$, $\omega_m(t) \in \mathbb{R}^3$ is the missile angular velocity control input, $d(t) \in \mathbb{R}^2$ is the unknown, generalized nonlinear disturbance (e.g., unmodeled effects), $J_\nu(p_t), J_\omega(p_t) \in \mathbb{R}^{2\times 3}$ denote the measurable image Jacobians given in Eq. (51) that relate the linear and angular velocities, respectively, of the missile and target to the target image velocity. Let the relative velocity $(\nu_m - \nu_t^m)$ be denoted by $\nu_r(t) \in \mathbb{R}^3$:

$$[J_\nu\ \ J_\omega] \triangleq \begin{bmatrix} -fa & 0 & u_t & \dfrac{u_t v_t}{fb} & -a\left(f + \dfrac{u_t^2}{fa^2}\right) & \dfrac{v_t a}{b} \\ 0 & -fb & v_t & b\left(f + \dfrac{v_t^2}{fb^2}\right) & -\dfrac{u_t v_t}{fa} & -\dfrac{u_t b}{a} \end{bmatrix} \tag{51}$$

Assumption 2. The unknown, generalized nonlinear disturbance $d(t)$ in Eq. (50) satisfies

$$\| d(t) \| \leq \gamma_0 \tag{52}$$

where $\gamma_0 \in \mathbb{R}$ is a known bounding constant and $\| \cdot \|_2$ denotes the vector 2-norm defined in Eq. (53).

Definition 1. The 2-norm of a vector-valued function $f(t) = \left[f_1(t), \ldots, f_n(t)\right]^T$ is given by

$$\| f \| = \left(\int_0^\infty \sum_{i=1}^{n} f_i^2(\tau)\, d\tau \right)^{1/2} = \left(\int_0^\infty f^T(\tau) f(\tau)\, d\tau \right)^{1/2} \tag{53}$$

For proportional navigation, we consider the *virtual* camera to be mounted at the origin of $\mathcal{F}_r$ defined in Eq. (49). Let $\mathcal{I}_v'$ denote the body-fixed non-rotating coordinate frame, coincident with $\mathcal{F}_r$, attached to this virtual camera. Following the development presented earlier, the image dynamics for $\mathcal{I}_v'$ can be obtained as

$$\dot{p}_t' = \frac{J_\nu}{z_t'}\left(\nu_m' - \nu_t^{m\prime}\right) + J_\omega \omega_m' + d \tag{54}$$

where $p_t'(t) \in \mathbb{R}^2$ are the virtual pixel coordinates corresponding to $\overline{m}_t'$ in Eq. (49) in the image

plane, $J_v(p_t'), J_\omega(p_t') \in \mathbb{R}^{2\times 3}$ are of the form (51), and $\nu_m'(t)$, $\nu_t^{m\prime}(t)$, and $\omega_m'(t)$ are the equivalent terms in Eq. (50) expressed in $\mathcal{I}_v'$. The pixel coordinates $p_t'(t)$ can be obtained from $\overline{m}_t'(t)$ using the pin-hole camera model, and the velocities $\nu_m'(t)$, $\omega_m'(t)$ in $\mathcal{I}_v'$ can be related to $\nu_m(t)$, $\omega_m(t)$ in $\mathcal{I}_v$ as

$$\begin{bmatrix} \nu_m \\ \omega_m \end{bmatrix} = \begin{bmatrix} R_m^m T R_o^m & \mathbf{0}^{3\times 3} \\ \mathbf{0}^{3\times 3} & R_m^m T R_o^m \end{bmatrix} \begin{bmatrix} \nu_m' \\ \omega_m' \end{bmatrix}. \tag{55}$$

where $\mathbf{0}^{n\times n}$ is a $n \times n$ matrix of zero elements.

5. Control objective

The control objective is to enable the missile airframe $\mathcal{F}_m$ to intercept a maneuvering target, or in a physical sense, to drive the relative distance between the missile and the target to zero. In this paper, we present a unified visual servo controller for pursuit guidance, parallel navigation, hybrid guidance by appropriately defining the control objective. In general, target interception can be achieved by regulating the time-varying target image coordinates $p_t(t)$ or $p_t'(t)$ to constant desired coordinates $p_d \in \mathbb{R}^2$. Therefore, mathematically, the control objective can be stated as

$$p_t(t) \to p_d \quad \text{or} \quad p_t'(t) \to p_d. \tag{56}$$

Specific control objective for each guidance law is defined below along with their merits and demerits.

Pursuit guidance: The target LOS vector $\hat{m}_t(t) \in \mathbb{R}^3$ expressed in $\mathcal{F}_m$ can be obtained as $\hat{m}_t = \overline{m}_t / \|\overline{m}_t\|$. Pursuit guidance requires that the missile velocity vector should coincide with the LOS vector. This objective can be achieved by steering the LOS vector $\hat{m}_t(t)$ along the optical axis of the camera $\mathcal{I}_v$, i.e., the longitudinal axis of the missile. Mathematically, by choosing $p_d = p_o$, the control objective becomes $p_t(t) \to p_o$, where $p_t(t)$ and p_o are defined in Section 4.

The pursuit guidance law is computationally less expensive than the proportional navigation and requires less communication bandwidth, since only the instantaneous target position $\overline{m}_t(t)$ is transmitted by $\mathcal{I}_m$ to the missile. However, pursuit guidance exhibits a tail-chasing behavior which may require more control energy.

Proportional navigation: The target LOS vector $\hat{m}_t'(t) \in \mathbb{R}^3$ expressed in $\mathcal{F}_r$ can be obtained as $\hat{m}_t' = \overline{m}_t' / \|\overline{m}_t'\|$. Proportional navigation is based on the principle of maintaining constant LOS relative to the inertial frame of reference, i.e., the LOS remains parallel to the initial LOS at all times. Let the initial LOS vector be denoted by $\hat{m}_t'(0)$ with the corresponding target position $\overline{m}_t'(0)$. Maintaining constant LOS in the inertial frame $\mathcal{F}_o$ is equivalent to maintaining constant LOS in $\mathcal{F}_r$. Therefore, the image coordinates corresponding to $\overline{m}_t'(0)$ in the virtual camera $\mathcal{I}_v'$ form the desired image coordinates, i.e.,

$$\begin{bmatrix} p_t'(0)^T & 1 \end{bmatrix}^T = \begin{bmatrix} p_d^T & 1 \end{bmatrix}^T = \frac{A_v' \overline{m}_t'(0)}{z_t'(0)} \tag{57}$$

and the control objective becomes $p_t'(t) \to p_d$, where p_t' is defined in Eq. (54), and $A_v' \in \mathbb{R}^{3\times 3}$ is a user-defined camera calibration matrix for the virtual camera $\mathcal{I}_v'$.

In proportional navigation, at each time, the camera $\mathcal{I}_m$ transmits the instantaneous target position $\overline{m}_t'(t)$ along with the orientation $R_o^m T(t) R_m^m(t)$ between $\mathcal{F}_m$ and $\mathcal{F}_r$ (see Eq. (55)) to the missile, thereby requiring additional communication bandwidth.

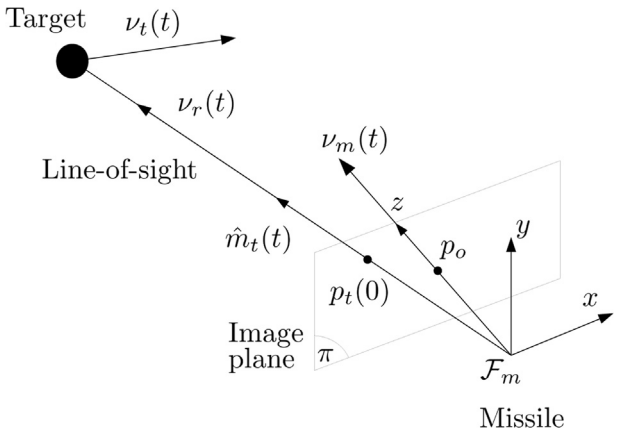

Fig. 3. 3D missile–target engagement geometry for hybrid guidance.

Hybrid guidance: In the proposed hybrid guidance, the objective is to maintain constant LOS in the missile body frame $\mathcal{F}_m$. For vision-based guidance, the constant LOS bearing condition can be satisfied by fixing the image-space coordinates of the target. Therefore, by choosing

$$\begin{bmatrix} p_t(0)^T & 1 \end{bmatrix}^T = \begin{bmatrix} p_d^T & 1 \end{bmatrix}^T = \frac{A_v \overline{m}_t(0)}{z_t(0)} \tag{58}$$

where $A_v \in \mathbb{R}^{3\times 3}$ is a user-defined camera calibration matrix for the virtual camera $\mathcal{I}_v$. The control objective in Eq. (56) can be written as $p_t(t) \to p_d$. The target will appear to be stationary in the image plane as the missile–target relative velocity $\nu_r(t)$ is directed along the line joining $p_t(0)$ with the origin of $\mathcal{F}_m$ as shown in Fig. 3.

The hybrid guidance only requires the instantaneous target position $\overline{m}_t(t)$, hence it has the same bandwidth usage as that of the pursuit guidance. Since the relative velocity is directed along the LOS vector in $\mathcal{F}_m$, the hybrid guidance does not exhibit significant tail-chasing behavior and requires less maneuvering than pursuit guidance.

6. Controller development

A unified visual servo controller is developed for the three guidance laws – pursuit guidance, parallel navigation, and hybrid guidance – to generate the angular rate commands for the missile. The error dynamics can be obtained by selecting the desired image coordinates p_d based on the respective control objective defined in Section 5. A polynomial approximation of the unknown relative velocity $\nu_r(t)$ will be used in the robust and adaptive elements of the guidance law that compensate for the uncertain and unmodeled dynamics.

A function $f(t)$ can be expressed in terms of a Taylor (or power) series, provided the function is continuous and suitably differentiable; and a polynomial approximation of $f(t)$ can be generated from truncation of its power series expansion as provided by the following lemma [1]:

Lemma 1. *If a continuous function $f(t)$ possesses a continuous $(n+1)$th derivative everywhere on the interval $[t_0, t]$, then it can be represented by a finite power series as*

$$f(t) = f(t_0) + \frac{(t-t_0)}{1!} f^{(1)}(t_0) + \cdots + \frac{(t-t_0)^{i-1}}{(i-1)!} f^{(i-1)}(t_0) + \cdots + \frac{(t-t_0)^n}{(n)!} f^{(n)}(t_0) + R(t) \tag{59}$$

where $f^{(i)}(\cdot)$ represents the ith time-derivative of the function $f(t)$ evaluated at the argument, and $R(t)$ denotes the remainder of Taylor formula given by

$$R(t) = \frac{(t-t_0)^{n+1}}{(n+1)!} f^{(n+1)}(\zeta), \quad t_0 < \zeta < t. \tag{60}$$

Based on the control objective, a regulation error $e(t) \in \mathbb{R}^2$, $e = [e_1 \; e_2]^T$, is defined as the difference between the target virtual image coordinates $p_t(t)$ (or $p_t'(t)$ for proportional navigation) and the constant desired image coordinates p_d as

$$e(t) \triangleq p_t(t) - p_d. \tag{61}$$

After taking the time-derivative of $e(t)$ and substituting the kinematic relationship given in Eq. (50) (or Eq. (54) for proportional navigation), the following expression can be obtained:

$$\dot{e} = \dot{p}_t = J_\nu \nu_r + J_\omega \omega_m + d \tag{62}$$

where the unknown scaled relative velocity $\nu_r(t)$ is assumed to be a continuously differentiable function of class c^p where the $(p+1)$ derivatives exist such that on any interval $[t_0, t]$ for $t \in [t_0, t_0 + T)$ it can be represented using Eq. (59), where $T \in \mathbb{R}$ is a constant interval length. Using Lemma 1, each element of $\nu_r(t)$ within a finite interval T can be represented locally at t_0 as a polynomial in time with unknown constant coefficients as [22]

$$\nu_r(t, t_0) = \begin{bmatrix} L(t,t_0) & \mathbf{0}^{p+1} & \mathbf{0}^{p+1} \\ \mathbf{0}^{p+1} & L(t,t_0) & \mathbf{0}^{p+1} \\ \mathbf{0}^{p+1} & \mathbf{0}^{p+1} & L(t,t_0) \end{bmatrix} \theta(t_0) + \delta_{\nu_r}(t, t_0) = \Delta(t, t_0)\theta(t_0)$$
$$+ \delta_{\nu_r}(t, t_0), \quad t \in [t_0, t_0 + T) \tag{63}$$

where $L(t, t_0) = [1 \; (t-t_0) \; \ldots \; (t-t_0)^p] \in \mathbb{R}^{1\times(p+1)}$ is a row vector of known functions of time. Also in Eq. (63), $\theta(t_0) \triangleq \left[\theta_x^T(t_0) \; \theta_y^T(t_0) \; \theta_z^T(t_0)\right]^T \in \mathbb{R}^{3(p+1)}$ denotes a vector of unknown coefficients, where $\theta_x(t_0)$, $\theta_y(t_0)$, $\theta_z(t_0) \in \mathbb{R}^{p+1}$ are obtained by evaluating the components of $\nu_r(t) \in \mathbb{R}^3$ and their first p derivatives locally at t_0, and $\delta_{\nu_r}(t, t_0) \in \mathbb{R}^3$ is a bounded function approximation error (i.e., the remainder from the Taylor series approximation). Note that $\theta(t_0)$ is only constant within each interval $[t_i, t_{i+1})$ and can differ from one interval to another for a time-varying parameter. For any non-negative constant $\beta \in \mathbb{R}$, the function approximation error $\delta_{\nu_r}(t, t_0)$ satisfies

$$\| \delta_{\nu_r}(t, t_0) \| \leq \beta \quad \forall t \geq 0. \tag{64}$$

It can be shown that $\delta_{\nu_r}(t, t_0)$ can be reduced by selecting a higher order polynomial (i.e., increasing p) and/or by reducing the interval length T. After substituting Eq. (63) in Eq. (62), the open-loop error system can be obtained as

$$\dot{e} = J_\nu(\Delta(t, t_0)\theta(t_0) + \delta_{\nu_r}(t, t_0)) + J_\omega \omega_m(t) + d. \tag{65}$$

The unknown relative velocity $\nu_r(t, t_0)$ measured in $\mathcal{F}_m$ can be estimated as

$$\hat{\nu}_r(t, t_0) = \Delta(t, t_0)\hat{\theta}(t_0) \tag{66}$$

where the time-varying estimate $\hat{\theta}(t) \in \mathbb{R}^{3(p+1)}$ of the unknown constant coefficient vector $\theta(t_0)$ is

designed using the following direct adaptive parameter update law:

$$\dot{\hat{\theta}} = \mathrm{proj}\left(\Gamma Y^T e\right). \tag{67}$$

In Eq. (67), the function proj(·) denotes a normal projection algorithm, which ensures that elements $\hat{\theta}_i(t) \forall i = 1, \ldots, 3(p+1)$ of $\hat{\theta}(t)$ are bounded as (for further details see [5,33])

$$\underline{\theta}_i \le \hat{\theta}_i(t) \le \overline{\theta}_i \tag{68}$$

where $\underline{\theta}_i$, $\overline{\theta}_i \in \mathbb{R}$ denote the known, constant lower and upper bounds, respectively, of $\hat{\theta}_i(t)$. In Eq. (67), $Y(p_t, t, t_0) = J_\nu \Delta$ is a known regression matrix, and $\Gamma \in \mathbb{R}^{3(p+1)\times 3(p+1)}$ is a diagonal, positive definite gain matrix. The adaptive update law given in Eq. (67) is designed for each time-interval of window size T, i.e., the coefficients $\theta(t_0)$ are considered to be constant during a given interval but may vary from one interval to the other. The relative velocity estimation error $\tilde{v}_r(t, t_0) \in \mathbb{R}^3$ is defined as

$$\tilde{v}_r(t, t_0) \triangleq \nu_r(t) - \hat{v}_r(t, t_0). \tag{69}$$

After substituting Eqs. (63) and (66) into Eq. (69), the relative velocity estimation error can be expressed as

$$\tilde{v}_r(t, t_0) = \Delta(t, t_0)\tilde{\theta}(t) + \delta_{\nu_r}(t, t_0) \tag{70}$$

where the estimation error $\tilde{\theta}(t) \in \mathbb{R}^{3(p+1)}$ is defined as

$$\tilde{\theta}(t) \triangleq \theta(t_0) - \hat{\theta}(t). \tag{71}$$

Remark 3. It can be shown that continuity of the estimate $\hat{\theta}(t, t_0)$ can be guaranteed during transitions between the ith and $(i+1)$th intervals by resetting the value of the estimate at the beginning of the $(i+1)$th interval for $i = 1, 2, \ldots$ as shown in Pagilla and Yu [22].

Based on the open-loop error system in Eq. (65) and the subsequent stability analysis, the missile angular velocity control input $\omega_m(t)$ can be designed as

$$\omega_m(t) = -J_\omega^+ \left(ke + Y\hat{\theta} + u_d\right). \tag{72}$$

Similar expression can be obtained in proportional navigation to get $\omega'_m(t)$, and Eq. (55) can be used to obtain $\omega_m(t)$ in $\mathcal{F}_m$. In Eq. (72), $J_\omega^+ \in \mathbb{R}^{3\times 2}$ denotes the Moore–Penrose right pseudo-inverse of the image Jacobian $J_\omega(p_t)$, $k \in \mathbb{R}^+$ is a control gain, and $u_d(t) \in \mathbb{R}^3$ is a robust feedback element designed to compensate for the function approximation error $\delta_{\nu_r}(t, t_0)$ and the bounded exogenous disturbance $d(t)$ as [4]

$$u_d(t) = \begin{cases} \left(\beta \|J_\nu\| + \gamma_0\right)\dfrac{e}{\|e\|}, & \|e\| > \epsilon_0 \\ \dfrac{1}{\epsilon_0}\left(\beta \|J_\nu\| + \gamma_0\right)e, & \|e\| \le \epsilon_0 \end{cases} \tag{73}$$

where $\epsilon_0 \in \mathbb{R}^+$, $\|J_\nu(p_t)\| \in \mathbb{R}$ is the induced matrix 2-norm as defined in Eq. (75), and $\gamma_0, \beta \in \mathbb{R}$ are defined in Eqs. (52) and (64), respectively. The advantages of the robust control term given in Eq. (73) are that it is a continuous feedback control, and that it can be tuned for precise target interception by selecting ϵ_0 arbitrarily small. After substituting the control input in Eq. (72) into

Eq. (65), the closed-loop error system can be obtained as

$$\dot{e} = -ke - u_d + Y\tilde{\theta} + J_v\delta_{v_r}(t, t_0) + d \tag{74}$$

where the property of pseudo-inverse matrix given in Remark 4 is used, and the condition to guarantee uniformly ultimately bounded system response is verified in Remark 5.

Remark 4. From the definition of $J_\omega(p_t)$ in Eq. (51), it can be seen that the rows of J_ω are linearly independent, i.e., J_ω is full row rank with rank equal to 2. Real, full row rank J_ω has right inverse $J_\omega^+ = J_\omega^T(J_\omega J_\omega^T)^{-1}$ with $J_\omega J_\omega^+ = I^{2\times 2}$, where I is an identity matrix.

Remark 5. The uncontrolled nominal system $(\delta_{vr}(t, t_0)) = d(t) = \omega_m(t) = 0)$ obtained from Eq. (62) as $\dot{e} = J_v\nu_r$ has no asymptotically stable equilibrium point. The new uncontrolled nominal system can be obtained by employing feedback $\omega_m(t)$. The new system $\dot{e} = -ke + Y\tilde{\theta}$ is asymptotically stable with $e=0$ as its only equilibrium point. Therefore, Assumption IV in [4] holds to guarantee uniformly ultimately boundedness of Eq. (74) using the robust feedback element (73).

Definition 2. The 2-norm of an $m \times n$ matrix A induced by the vector norm is given by

$$\|A\| = \max_{\mathbf{x}\neq 0} \frac{\|A\mathbf{x}\|}{\|\mathbf{x}\|} = \max_{\|\mathbf{x}\|=1} \|A\mathbf{x}\| \tag{75}$$

where $\mathbf{x} \in \mathbb{K}^n$ is defined over a real or complex field.

7. Controller characteristics

7.1. Stability analysis

Theorem 1. *The adaptive IBVS guidance law of Eqs.* (67), (72) *and* (73) *ensures uniformly ultimately bounded target image tracking in the sense that*

$$\|e(t)\| \leq \zeta_0 \exp\{-\zeta_1 t\} + \zeta_2 \tag{76}$$

where $\zeta_0, \zeta_1, \zeta_2 \in \mathbb{R}$ *denote positive bounding constants.*

Proof. Let $V(t) \in \mathbb{R}$ be defined as the following nonnegative function during each interval $t \in [t_i, t_{i+1})$:

$$V = \tfrac{1}{2}e^T e + \tfrac{1}{2}\tilde{\theta}^T\Gamma^{-1}\tilde{\theta}. \tag{77}$$

Based on Eqs. (68) and (71), the Lyapunov function in Eq. (77) can be upper and lower bounded as

$$\lambda_1\|e\|^2 + c_1 \leq V(t) \leq \lambda_2\|e\|^2 + c_2 \tag{78}$$

where $\lambda_1, \lambda_2, c_1, c_2 \in \mathbb{R}$ are known positive bounding constants. After using Eqs. (67) and (74),

the time-derivative of $V(t)$ can be expressed as

$$\dot{V} = -e^T k e - e^T u_d + e^T (J_\nu \delta_{\nu_r}(t, t_0) + d). \tag{79}$$

Thus, from Eq. (73), if $\|e\| > \epsilon_0$, $\dot{V}(t)$ can be upper bounded as

$$\dot{V} \leq -k\|e\|^2 - (\beta\|J_\nu\| + \gamma_0)\|e\| + \left(\|\delta_{\nu_r}(t, t_0)\|\,\|J_\nu\| + \|d\|\right)\|e\|. \tag{80}$$

After canceling common terms and using the bounds on $d(t)$ and $\delta_{\nu_r}(t, t_0)$ defined in Eqs. (52) and (64), respectively, the upper bound in Eq. (80) can be rewritten as

$$\dot{V} \leq -k\|e\|^2. \tag{81}$$

From Eqs. (77) and (81), it is clear that $e(t), \tilde{\theta}(t) \in \mathcal{L}_\infty$ and that $e(t) \in \mathcal{L}_2$. Using Eq. (61) and the fact that $e(t) \in \mathcal{L}_\infty$, the image coordinates $p_t(t) \in \mathcal{L}_\infty$, and therefore image Jacobians $J_\nu(u_t, v_t)$, $J_\omega(u_t, v_t) \in \mathcal{L}_\infty$ along with $Y(u_t, v_t, t, t_0) \in \mathcal{L}_\infty$. Given that $e(t) \in \mathcal{L}_\infty$, Eqs. (64), (67), (68), (72) and (73) can be used along with Assumption 1 and Remark 4 to prove that the control inputs $\hat{\theta}(t)$, $u_d(t)$, $\omega_m(t) \in \mathcal{L}_\infty$.From $\tilde{\theta}(t) \in \mathcal{L}_\infty$, $\delta_{\nu_r}(t, t_0)$, $d(t) \in \mathcal{L}_2$ and using the above facts, $\dot{e}(t) \in \mathcal{L}_\infty$, and hence $e(t)$ is uniformly continuous. Based on the fact that $e(t)$, $\dot{e}(t) \in \mathcal{L}_\infty$ and $e(t) \in \mathcal{L}_2$, a corollary to Barbalat's Lemma can be used to prove that the error $e(t)$ asymptotically enters a ball of radius ϵ_0 centered at the origin $e = \mathbf{0}$[2].

For the case when $\|e\| \leq \epsilon_0$, the expression in Eq. (79) can be upper bounded as

$$\dot{V} \leq -k\|e\|^2 - \frac{1}{\epsilon_0}\left(\beta\|J_\nu\| + \gamma_0\right)\|e\|^2 + \left(\|\delta_{\nu_r}(t, t_0)\|\,\|J_\nu\| + \|d\|\right)\|e\|. \tag{82}$$

Using the upper bound in Eqs. (52) and (64), and after completing the squares in Eq. (82), the upper bound on $\dot{V}(t)$ can be expressed as

$$\dot{V} \leq -k\|e\|^2 + \tfrac{1}{4}\left(\beta\|J_\nu\| + \gamma_0\right)\epsilon_0. \tag{83}$$

Writing the Jacobian $J_\nu = J_\nu' + J_\nu''$, where $J_\nu'(p), J_\nu'' \in \mathbb{R}^{2\times 3}$ are the following rank deficient matrices:

$$J_\nu' = \begin{bmatrix} u_t & 0 & 0 \\ v_t & 0 & 0 \end{bmatrix}, \quad J_\nu'' = \begin{bmatrix} 0 & -fa & 0 \\ 0 & 0 & fb \end{bmatrix}. \tag{84}$$

Using the property $\|J_\nu\| \leq \|J_\nu'\| + \|J_\nu''\|$ and from the induced norm definition in Eq. (75), for $\mathbf{x} = [1\ 0\ 0]^T$, $\max_{\|\mathbf{x}\|=1}\|J_\nu'\mathbf{x}\| = \|p_t\|$. Therefore, using Eq. (61) and the fact that $\|e\| \leq \epsilon_0$, the inequality in Eq. (83) can be written as

$$\dot{V} \leq -k\|e\|^2 + \tfrac{1}{4}\left(\beta\epsilon_0 + \beta\|p_d\| + \beta\|J_\nu''\| + \gamma_0\right)\epsilon_0. \tag{85}$$

Consequently, for all $(e, t) \in \mathbb{R}^2 \times \mathbb{R}$, Eq. (78) can be used to express inequality (85) as

$$\begin{aligned} \dot{V} &\leq -\frac{k}{\lambda_2} V(t) + \zeta_1 \\ \zeta_1 &= \frac{kc_2}{\lambda_2} + \frac{1}{4}\left(\beta\epsilon_0 + \beta\|p_d\| + \beta\|J_\nu''\| + \gamma_0\right)\epsilon_0 \end{aligned} \tag{86}$$

where $\zeta_1 \in \mathbb{R}^+$ is a constant. The linear differential inequality in Eq. (86) can be solved as

$$V(t) \leq \exp\left\{-\frac{k}{\lambda_2}t\right\}V(0) + \zeta_1\frac{\lambda_2}{k}\left(1 - \exp\left\{-\frac{k}{\lambda_2}t\right\}\right). \tag{87}$$

The expressions in Eqs. (77), (78) and (86) can be used to conclude that $e(t), \tilde{\theta}(t) \in \mathcal{L}_\infty$. Using identical signal chasing arguments as presented above, it can be concluded that $\dot{e}(t) \in \mathcal{L}_\infty$. The

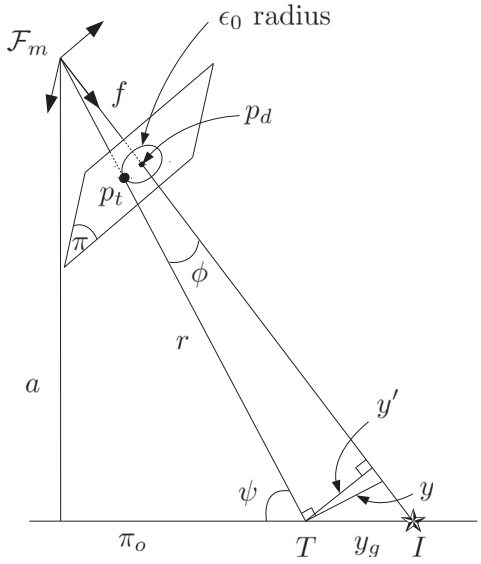

Fig. 4. Relationship between the ground and image planes.

inequalities in Eqs. (78) and (87) can be used to conclude that

$$\|e\|^2 \leq \frac{\left(\lambda_2 \|e(0)\|^2 + c_2\right)}{\lambda_1} \exp\left\{-\frac{k}{\lambda_2}t\right\} + \left(\frac{\zeta_1\lambda_2}{\lambda_1 k} + \frac{c_2 - c_1}{\lambda_1}\right) < \gamma_1 \|e(0)\| \tag{88}$$

where $\gamma_1 \in \mathbb{R}^+$ is a constant. The result in Eq. (76) can now be directly obtained from Eq. (88). Thus, the robust term designed in Eq. (73) guarantees uniform ultimate bounded target image regulation, where the error bound can be reduced by selecting arbitrarily small ϵ_0 [4]. Hence, the target image coordinates are regulated within a small region centered at desired pixel coordinates p_d.□

7.2. Miss distance

The miss distance is defined as the closest point of approach of the missile with respect to the target [25], which represents the error in positioning the missile with respect to the target assuming the missile and the target do not maneuver in future. Fig. 4 shows the impact geometry by considering the relationship between ground and image planes, where T denotes the target location, and I is the impact point. The objective is to determine the miss distance $y(t) \in \mathbb{R}$ perpendicular to the LOS in terms of the target image coordinates. The miss distance can subsequently be used to determine the range error $y_g(t)$ along the ground and the zero-effort miss.

From Fig. 4, the following expressions can be obtained:

$$\tan\phi = \frac{\|p_t\|}{f}, \quad \psi = \sin^{-1}\left(\frac{a}{r}\right), \quad y' = \frac{\|p_t\| r \cos\phi}{f} \tag{89}$$

where $a(t) \in \mathbb{R}$ is the missile altitude above plane π_o, $r(t) \in \mathbb{R}$ denotes the range to the target, and f is the user-defined focal length of the respective virtual camera. Using Eq. (89), the miss

distance and the range error can be obtained as

$$y = \frac{y'}{\cos\ \phi} = \frac{\|p_t\| r}{f} \tag{90}$$

$$y_g = \frac{y\ \cos\ \phi}{\sin(\psi - \phi)}. \tag{91}$$

Substituting Eq. (90) in the first expression from Eq. (89) and taking the time derivative we get

$$\dot{\phi} = \frac{\dot{y} t_{\text{go}} + y}{\nu_{cl} t_{\text{go}}^2\ \sec^2\ \phi} \tag{92}$$

where $\nu_{cl} \in \mathbb{R}$ is the constant closing velocity assuming that the missile and target do not maneuver in future, and $t_{\text{go}} \in \mathbb{R}$ is the time-to-go until the end of the flight. From Eq. (92), the zero-effort miss $y_z(t) \in \mathbb{R}$ can be obtained by substituting the time derivative of $y(t)$ along with Eq. (90) and canceling the common terms as

$$y_z = \frac{\hat{p}_t^T \dot{p}_t \nu_{cl} t_{\text{go}}^2}{f} \tag{93}$$

where $\hat{p}_t(t) \in \mathbb{R}^2$ is a unit vector along $p_t(t)$ in the image plane of the virtual camera. Substituting the image dynamics in Eq. (50) into Eq. (93), an upper-bound on the zero-effort miss for the developed pursuit and hybrid guidance laws can be obtained as below:

$$y_z \leq \frac{\|J_\nu\| \nu_{cl} t_{\text{go}}}{f\ \cos\ \phi} \tag{94}$$

where the following facts are used: $\omega_m(t) = \mathbf{0}^3$ as the missile does not maneuver in future, $\|\nu_m - \nu_t^m\|$ is the constant closing velocity ν_{cl}, and the target depth $z_t = r\ \cos\ \phi$. Using Eqs. (61) and (84), the upper-bound on $y_z(t)$ can be evaluated as

$$y_z \leq \frac{\|e\| \nu_{cl} t_{\text{go}} + \|p_d\| \nu_{cl} t_{\text{go}} + fa \nu_{cl} t_{\text{go}}}{f\ \cos\ \phi}. \tag{95}$$

In Eq. (95), the induced norm $\|J_\nu'\| = \|p_t\|$ for $\mathbf{x} = [1\ 0\ 0]^T$ and $\|J_\nu''\| = fa$ for $\mathbf{x} = [0\ 0\ 1]^T$ when $a = b$ in Eq. (84). It can be seen that the zero-effort miss is a function of the regulation error $e(t)$. For the controller (67), (72), and (73) developed in Section 6, when the error $\|e(t)\| \leq \epsilon_0$, an upper bound on the zero-effort miss can be obtained as

$$\textbf{Pursuit guidance} \quad y_z \leq \frac{\nu_{cl} t_{\text{go}}}{f\ \cos\ \phi} \left(\epsilon_0 + \|p_o\| + fa\right) \tag{96}$$

$$\textbf{Hybrid guidance} \quad y_z \leq \frac{\nu_{cl} t_{\text{go}}}{f \cos\phi} \left(\epsilon_0 + \frac{\|A_v\|}{\cos\phi_0} + fa\right) \tag{97}$$

where $\phi_0 \in \mathbb{R}$ is the LOS to the target in $\mathcal{F}_m$ at time $t = 0$.

To determine the zero-effort miss for proportional navigation, the following expression can be obtained from Eq. (49) that relates the pixel coordinates $p_t(t)$ in $\mathcal{I}_v$ to $p_t'(t)$ in $\mathcal{I}_v'$:

$$\begin{bmatrix} p_t \\ 1 \end{bmatrix} = \frac{z_t'}{z_t} A_v R_m^{mT} R_o^m A_v' - 1 \begin{bmatrix} p_t' \\ 1 \end{bmatrix}. \tag{98}$$

Since $w_m(t) = \mathbf{0}^3$, the rotation $R_m^{mT} R_o^m$ of $\mathcal{F}_m$ with respect to $\mathcal{F}_o$ is constant. Substituting the time-

derivative of Eq. (98) into Eq. (93), the zero-effort miss can be obtained as

$$y_z = \begin{bmatrix}\hat{p}_t^T & 0\end{bmatrix}\frac{z_t' t_{\mathrm{go}}}{f\ \cos\ \phi}A_v R_m^{mT} R_o^m A_v' - 1\begin{bmatrix}\hat{p}_t'^T & 0\end{bmatrix}^T - \begin{bmatrix}\hat{p}_t^T & 0\end{bmatrix}\frac{[0\ 0\ 1]^T R_o^{mT} R_m^m (\nu_m - \nu_t^m) t_{\mathrm{go}}}{f\ \cos\ \phi}A_v R_m^{mT} R_o^m A_v'$$

$$-1\begin{bmatrix}p_t'^T & 1\end{bmatrix}^T + \begin{bmatrix}\hat{p}_t^T & 0\end{bmatrix}\frac{z_t'[0\ 0\ 1]^T(\nu_m - \nu_t^m)}{f\nu_{cl}\ \cos^2\phi}A_v R_m^{mT} R_o^m A_v' - 1\begin{bmatrix}p_t'^T & 1\end{bmatrix}^T. \tag{99}$$

Using Eq. (54) with $\omega_m(t) = \mathbf{0}^3$ and $d(t) = \mathbf{0}^2$, and canceling common terms, the expression in Eq. (99) can be simplified as

$$y_z = \begin{bmatrix}\hat{p}_t^T & 0\end{bmatrix}\frac{t_{\mathrm{go}}}{f\ \cos\ \phi}A_v R_m^{mT} R_o^m A_v' - 1\tilde{J}_\nu R_o^{mT} R_m^m (\nu_m - \nu_t^m) \tag{100}$$

where $\tilde{J}_\nu(u_t', v_t') \in \mathbb{R}^{3\times 3}$ is the following Jacobian:

$$\tilde{J}_\nu = \tilde{J}_\nu' + \tilde{J}_\nu'' = \begin{bmatrix} -f'a' & 0 & u_t' \\ 0 & -f'b' & v_t' \\ 0 & 0 & 0 \end{bmatrix} \tag{101}$$

$$\tilde{J}_\nu' = \begin{bmatrix} 0 & 0 & u_t' \\ 0 & 0 & v_t' \\ 0 & 0 & 0 \end{bmatrix}, \quad \tilde{J}_\nu'' = \begin{bmatrix} -f'a' & 0 & 0 \\ 0 & -f'b' & 0 \\ 0 & 0 & 0 \end{bmatrix} \tag{102}$$

where $f', a', b' \in \mathbb{R}$ are camera calibration parameters of the virtual camera attached to $\mathcal{I}_v'$. From Eqs. (100) to (102), an upper-bound on $y_z(t)$ can be obtained as

$$y_z \le \frac{\nu_{cl} t_{\mathrm{go}}}{f\ \cos\ \phi}\|A_v\|\,\|A_v' - 1\|\left(\|p_t'\| + f'a'\right) \tag{103}$$

where the fact that the spectral norm of orthogonal matrices $\|R_m^{mT} R_o^m\|_2 = \|R_o^{mT} R_m^m\|_2 = 1$ is used. Also, the induced norm of $\|\tilde{J}_\nu'\| = \|p_t'\|$ for $\mathbf{x} = [0\ 0\ 1]^T$ and $\|\tilde{J}_\nu\| = f'a'$ for $\mathbf{x} = [1\ 0\ 0]^T$ when $a' = b'$ in Eq. (101). Therefore, an upper-bound on the zero-effort miss distance for proportional navigation can be obtained as

$$\textbf{Proportional navigation} \quad y_z \le \frac{\nu_{cl} t_{\mathrm{go}}}{f\ \cos\ \phi}\|A_v\|\,\|A_v' - 1\|\left(\epsilon_0 + \frac{\|A_v'\| r}{\varepsilon} + f'a'\right) \tag{104}$$

where $\varepsilon \in \mathbb{R}^+$, such that $z_t'(0) > \varepsilon$.

8. Simulation results

This section describes the results of a numerical simulation to demonstrate the performance of the proposed vision-based relative navigation and control approach for a sensorless missile. The simulation scenario consists of a ground target represented as a point object that is moving in a plane containing the reference object $\mathcal{F}_o$. The moving camera $\mathcal{I}_m$ can view the missile, whereas another moving camera $\mathcal{I}_t$ tracks the ground target. The motion of the target as well as cameras is unknown for control purposes. The target to be intercepted is considered to undergo different maneuvers, namely evasive maneuver, step maneuver, and stop-and-go maneuver. Evasive maneuver is continuously differentiable, whereas step and stop-and-go maneuvers are piecewise

continuous in time. For each case, the missile control problem is formulated in terms of pursuit guidance, parallel navigation, and hybrid guidance.

8.1. Missile and reference object

The position $t_m \in \mathbb{R}^3$ and orientation $R_m \in \mathbb{SO}^3$ of the missile body frame $\mathcal{F}_m$ with respect to the ESF reference frame $\mathcal{F}_e$ at time $t=0$ was considered to be

$$t_m = [300 \;\; 400 \;\; -2000]^T \text{ m}$$
$$R_m = \begin{bmatrix} 0.8529 & -0.3966 & 0.3396 \\ 0.1504 & 0.8095 & 0.5676 \\ -0.5000 & -0.4330 & 0.7500 \end{bmatrix} \tag{105}$$

which also represents the pose of the stationary reference missile frame $\mathcal{F}_{rm}$. The unknown time-varying linear velocity $\nu_m \in \mathbb{R}^3$ of the missile in body frame $\mathcal{F}_m$ was assumed to be

$$\nu_m = [0 \;\; 0 \;\; 250 - 20\sin(0.01t)]^T \text{ m/s}. \tag{106}$$

A nonlinear bounded disturbance $d_m(t) \in \mathbb{R}^3$, e.g., due to wind gust or atmospheric disturbance, is assumed to perturb the missile position between time interval $1.2\text{ s} \le t \le 1.8\text{ s}$. The disturbance in the missile position results in the corresponding disturbance $d(t)$ in the target image velocity.

The position $t_o \in \mathbb{R}^3$ and orientation $R_o \in \mathbb{SO}^3$ of the stationary reference object with respect to $\mathcal{F}_e$ was selected as

$$t_o = [500 \;\; 1500 \;\; 0]^T \text{ m}, \quad R_o = I^{3\times 3}. \tag{107}$$

8.2. Cameras

The position $t_{cm} \in \mathbb{R}^3$ and orientation $R_{cm} \in \mathbb{SO}^3$ of the time-varying camera coordinate frame $\mathcal{I}_m$ with respect to $\mathcal{F}_e$ at $t=0$ was assumed to be

$$t_{cm} = [400 \;\; 900 \;\; -3000]^T \text{ m}, \quad R_{cm} = I^{3\times 3} \tag{108}$$

where $I^{3\times 3}$ denotes an identity matrix. The reference camera coordinate frame $\mathcal{I}_r$ is assumed to be located at the initial pose (t_{cm}, R_{cm}) of $\mathcal{I}_m$ given in Eq. (108). The time-varying linear $\nu_{cm}(t) \in \mathbb{R}^3$ and angular $\omega_{cm} \in \mathbb{R}^3$ velocity of the camera measured in body frame $\mathcal{I}_m$ was

$$\nu_{cm} = [120 \;\; 60 \;\; 20\sin(t)]^T \text{ m/s} \tag{109}$$

$$\omega_{cm} = [0.1 \;\; 0 \;\; 0.12]^T \text{rad/s}. \tag{110}$$

Similarly, the position $t_{ct} \in \mathbb{R}^3$ and orientation $R_{ct} \in \mathbb{SO}^3$ of the time-varying camera coordinate frame $\mathcal{I}_t$ with respect to $\mathcal{F}_e$ at $t=0$ was assumed to be

$$t_{ct} = [1100 \;\; 1600 \;\; -1000]^T \text{ m}, \quad R_{ct} = I^{3\times 3}. \tag{111}$$

The time-varying linear $\nu_{ct}(t) \in \mathbb{R}^3$ and angular velocity $\omega_{ct} \in \mathbb{R}^3$ of the camera measured in body frame $\mathcal{I}_t$ was

$$\nu_{ct} = [60 \;\; 60 \;\; 30\sin(t)]^T \text{ m/s} \tag{112}$$

$$\omega_{ct} = [0.05 \;\; 0 \;\; 0.4]^T \text{ rad/s}. \tag{113}$$

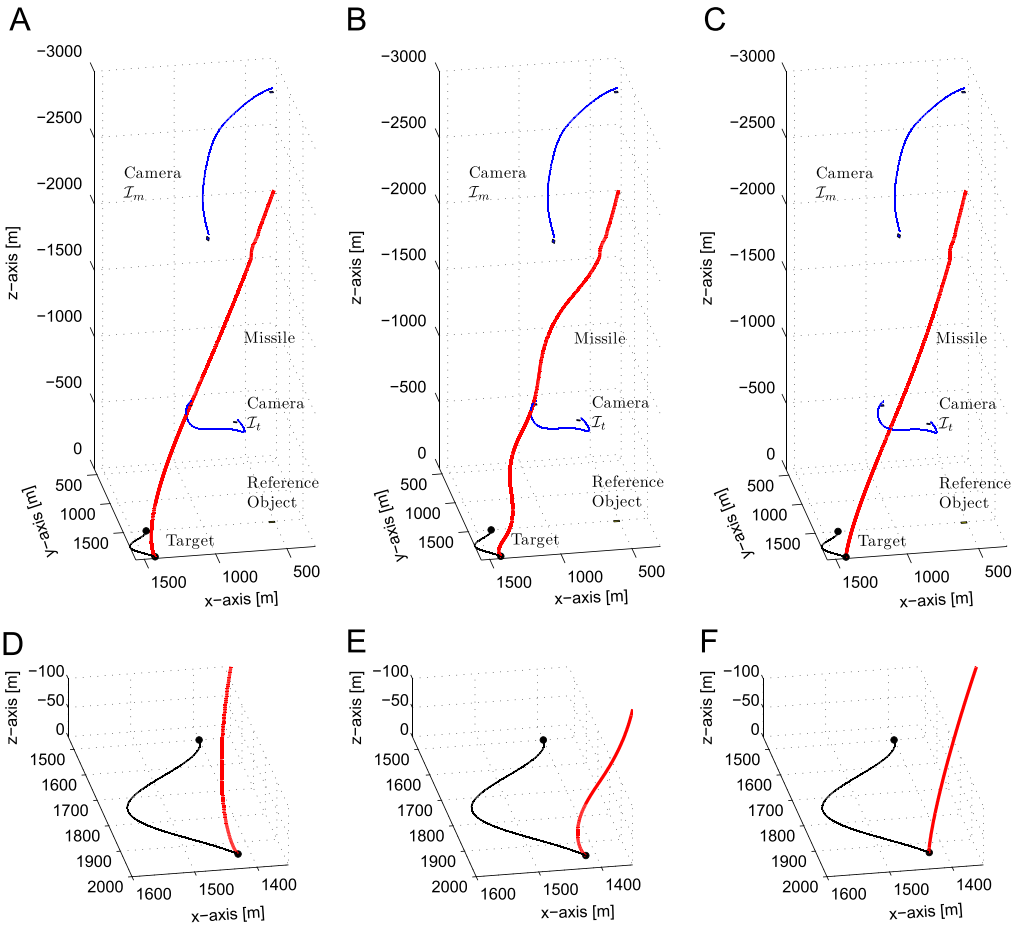

Fig. 5. Euclidean plots showing missile, target, and camera trajectories for (A) pursuit guidance, (B) proportional navigation, and (C) hybrid guidance, where the target is performing continuous evasive maneuvers. The details of the target motion along with the missile trajectory at impact are shown in (D), (E) and (F) for the respective guidance laws.

8.3. Target

The position $t_t \in \mathbb{R}^3$ of the time-varying point target with respect to $\mathcal{F}_e$ at $t=0$ was assumed to be

$$t_t = [1400 \;\; 1500 \;\; 0]^T \text{ m}. \tag{114}$$

Various target motion scenarios are described below.

8.3.1. Evasive maneuver

The target is performing evasive maneuvers with unknown time-varying acceleration (see Fig. 5(a)), where the time-varying velocity $\nu_t(t) \in \mathbb{R}^3$ of the target measured in $\mathcal{F}_e$ was assumed

to be a class C^{∞} (smooth) function as

$$\nu_t = [40\ \sin(0.5t)\ \ 40\ \ 0]^T \text{ m/s}. \tag{115}$$

8.3.2. Step maneuver

The target is considered to move with an unknown constant velocity parallel to the x- or the y-axis of $\mathcal{F}_e$ with aperiodic switching as shown in Fig. 5(b) to represent an adversary navigating an urban environment. The velocity $\nu_t(t)$ can be written as

$$\nu_t = \begin{cases} [\pm 40\ \ 0\ \ 0]^T \text{ m/s}, & t_i \le t < t_{i+1}, \\ [0\ \ \pm 40\ \ 0]^T \text{ m/s}, & t_{i+1} \le t < t_{i+2} \end{cases} \tag{116}$$

where $t_i \in \mathbb{R}$ denote the time instances when the direction of motion of the target changes, and $i = 1, 3, 5, \ldots$. In Eq. (116), the velocity $\nu_t(t)$ is a piecewise smooth function with a jump discontinuity at t_i.

8.3.3. Stop-and-go maneuver

The target is considered to undergo a stop-and-go motion as shown in Fig. 5(c) where the unknown time-varying velocity $\nu_t(t)$ of the target is given by

$$\nu_t = \begin{cases} [40\sin(0.5t)\ \ 40\ \ 0]^T \text{ m/s}, & t_i \le t < t_{i+1} \\ [0\ \ 0\ \ 0]^T \text{ m/s}, & t_{i+1} \le t < t_{i+2}. \end{cases} \tag{117}$$

The considered stop-and-go motion is piecewise smooth and discontinuous with a jump discontinuity. The discontinuity occurs at random start and stop points at times t_i, $\forall i = 1, 2, \ldots$.

The simulation results described in this section assume that the image measurements (pixel coordinates) of the missile, target, and reference object, $p_m(t)$, $p_t(t)$, $p_o(t)$, respectively, are affected by an additive white Gaussian noise of standard deviation 0.1 pixels. The mathematical models for the missile linear velocity, camera velocity, and target maneuvers given in Eqs. (106), (109), (110), (112), (113) and (115)–(117) are used to generate the plant model only; they are not used in the guidance law. Also, the pose of the missile, camera, target, and reference object given in Eqs. (105), (107), (108), (111) and (114) are not available to the controller.

Figs. 5–7 show the results of the developed vision-based navigation and control approach using the guidance objectives defined in Section 5 for target undergoing evasive maneuvers, stop-and-go maneuvers, and step maneuvers, respectively. The Euclidean trajectories of the missile ($\mathcal{F}_m$), cameras ($\mathcal{I}_m$ and $\mathcal{I}_t$), and target are shown in Figs. 5–7 along with the details at impact. To compare the performance of different guidance laws, Fig. 8 shows missile trajectories in the xy-plane. In Fig. 8, pursuit guidance exhibits the well-known tail-chasing behavior, proportional guidance without the knowledge of the target acceleration (i.e., no APNG) results in excessive missile maneuvers, whereas hybrid guidance is observed to perform well in the presence of a maneuvering target. Hybrid guidance has limitation in non-maneuvering target scenarios (e.g., target moving in a straight line) as increased missile maneuvers will be required to maintain constant LOS in the missile body frame. In such cases, the presented vision-based navigation and control approach can be used with pursuit guidance or proportional navigation. The plot of the regulation error $e(t)$ for continuous target maneuvers is shown in Fig. 9. It is to be

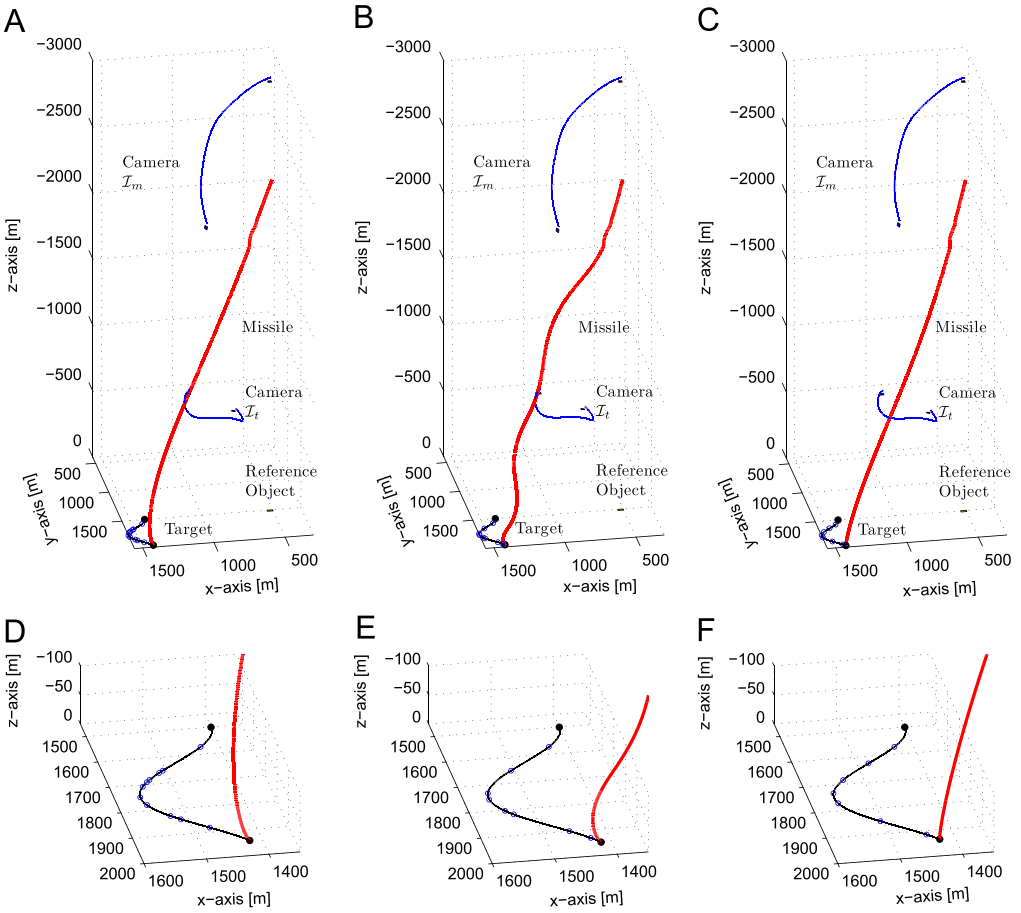

Fig. 6. Euclidean plots showing missile, target, and camera trajectories for (A) pursuit guidance, (B) proportional navigation, and (C) hybrid guidance, where the target is performing piecewise continuous stop-and-go maneuvers. The details of the target motion along with the missile trajectory at impact are shown in (D), (E) and (F) for the respective guidance laws.

noted that the target pixel coordinates are measured in the virtual camera $\mathcal{I}_v$ for pursuit and hybrid guidance and $\mathcal{I}_v'$ for proportional navigation. The error $e(t)$ remains bounded during the closed-loop operation of the system, and since the virtual camera is assumed to be at the origin of $\mathcal{F}_m$, the error becomes large at the impact as $z_t(t)$ (or $z_t'(t)$) goes to zero. In practice, the virtual camera frame will be defined by taking into account the size of the ballistic (refer to Remark 2). The robust feedback element in the control structure compensates for the nonlinear disturbance and hence, no perturbation other than due to image noise in $e(t)$ can be observed during $1.2\text{ s} \leq t \leq 1.8\text{ s}$. Fig. 10 shows LOS vectors for the different guidance laws. It can be observed in Fig. 10(a) that in pursuit guidance the LOS vector is regulated to coincide with the optical axis of the virtual camera (i.e., along the longitudinal or z-axis of the missile frame $\mathcal{F}_m$), while for hybrid guidance the LOS vector remains constant in $\mathcal{F}_m$. For proportional navigation, the LOS

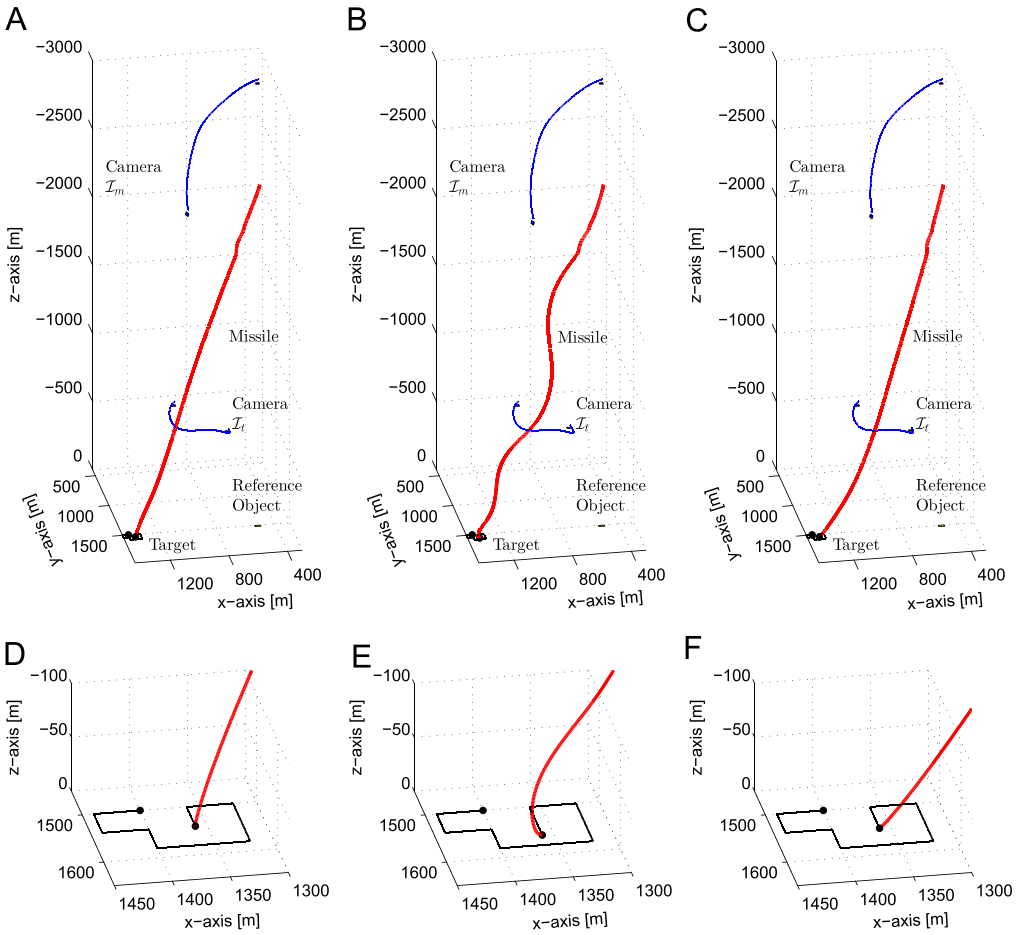

Fig. 7. Euclidean plots showing missile, target, and camera trajectories for (A) pursuit guidance, (B) proportional navigation, and (C) hybrid guidance, where the target is performing piecewise continuous step maneuvers. The details of the target motion along with the missile trajectory at impact are shown in (D), (E) and (F) for the respective guidance laws.

vector remains constant in $\mathcal{I}_v'$ (i.e., parallel to the initial LOS in the ESF frame $\mathcal{F}_e$) as shown in Fig. 10(b). The average miss distance and time to intercept the target for pursuit guidance, proportional navigation, and hybrid guidance based on 100 Monte Carlo trials are given in Table 2. The proposed vision-based navigation and control strategy using distributed off-board sensing achieves target interception with a reasonable miss distance (<1 m).

9. Conclusions

The framework for vision-based navigation and control of a sensorless missile is presented. Off-board vision sensors employing the daisy-chaining methodology solve the three-dimensional

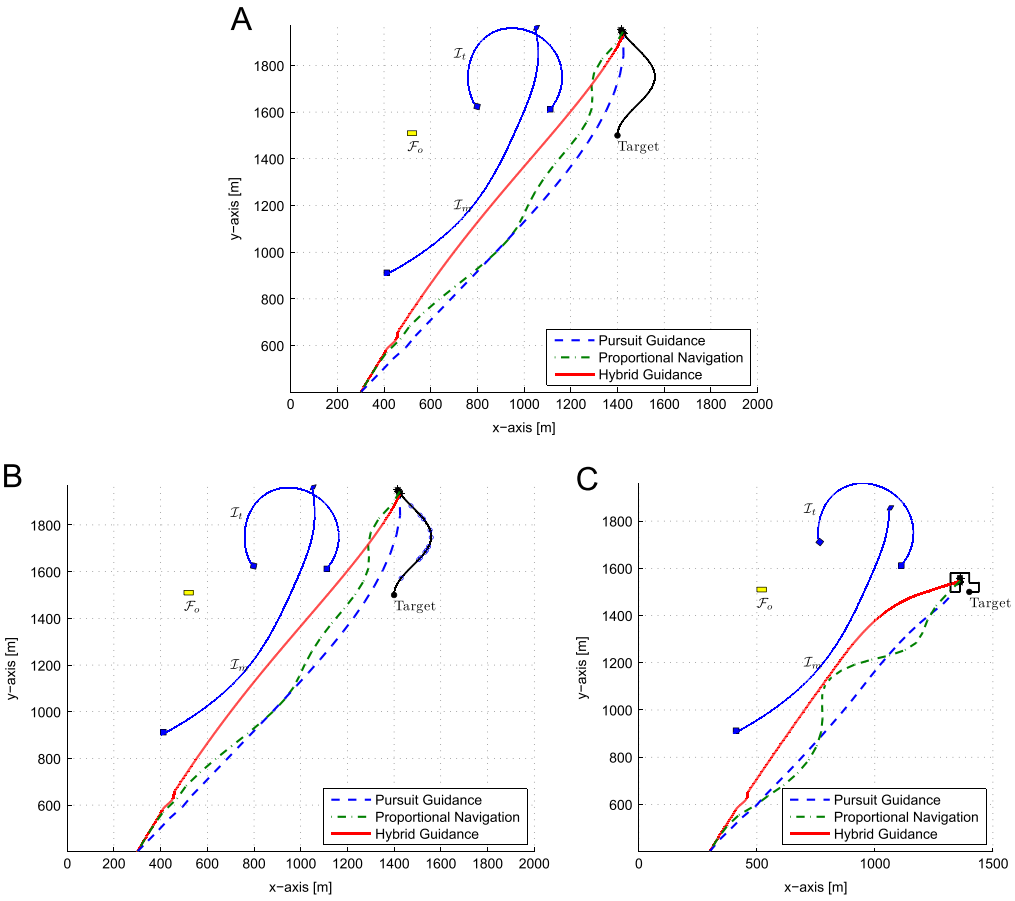

Fig. 8. Missile, target, and camera trajectories in the xy-plane of $\mathcal{F}_e$ for the target moving with (A) evasive maneuvers, (B) stop-and-go maneuvers, and (C) step maneuvers.

Euclidean reconstruction problem to obtain the unknown time-varying target position. To account for the unknown target maneuvers and the lack of on-board sensing, the target dynamics are expressed in a virtual camera attached to the missile. Apart from formulating pursuit guidance and parallel navigation in vision-based framework, we introduced a hybrid guidance law that is shown to perform well in intercepting a maneuvering target. A unified visual servo controller is developed for pursuit guidance, proportional navigation, and the proposed hybrid guidance by appropriately defining the control objective.

There are several avenues of future work. One is to relax the assumption of known geometric length on the missile by developing a nonlinear observer by considering known velocity of the camera $\mathcal{I}_m$. Available communication bandwidth plays an important role in the stability of networked control systems. Another exciting avenue is to analyze the effect of communication bandwidth on the miss distance and develop a stabilizing missile guidance law in the presence of bandwidth limitations.

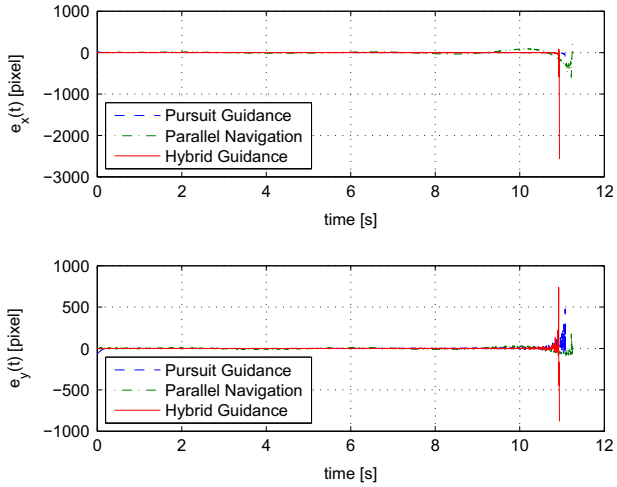

Fig. 9. Regulation error $e(t) \triangleq \left[e_x(t)\ e_y(t)\right]^T$ of the target pixel coordinates measured in the virtual camera $\mathcal{I}_v$ for pursuit and hybrid guidance, and $\mathcal{I}_v'$ for proportional navigation when the target undergoes continuous evasive maneuvers.

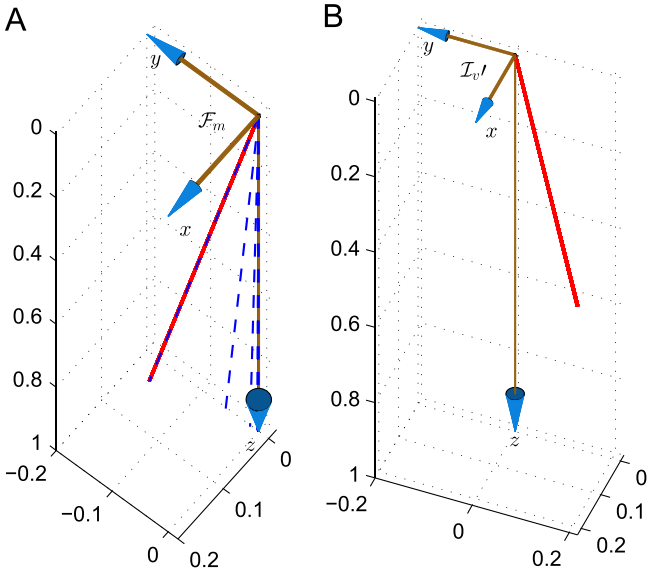

Fig. 10. (A) LOS vectors in pursuit guidance and hybrid guidance (i.e., $\hat{m}(t)\ \forall t$ expressed in $\mathcal{I}_v$ or $\mathcal{F}_m$) shown in dotted blue lines and solid red line, respectively. (B) LOS vectors in proportional navigation (i.e., $\hat{m}'(t)\ \forall t$ expressed in $\mathcal{I}_v'$, which has the same orientation as $\mathcal{F}_e$) shown in solid red line. (For interpretation of the references to color in this figure caption, the reader is referred to the web version of this paper.)

Table 2
Expected miss distance and time to intercept the target based on 100 Monte Carlo trials.

Maneuver	**Pursuit guidance**		**Proportional navigation**		**Hybrid guidance**	
	Miss distance (m)	Time (s)	Miss distance (m)	Time (s)	Miss distance (m)	Time (s)
Evasive	1.2932	11.11	1.7880	11.28	0.8438	10.94
Stop-and-go	1.2405	10.92	1.8414	11.27	0.4034	10.79
Step	1.1518	10.01	2.2151	10.48	0.8502	10.12

References

[1] B. Carnahan, H. Luther, J. Wilkes, Applied Numerical Methods, John Wiley & Sons Inc., New York, 1969.
[2] H. Chen, K. Chang, C.S. Agate, UAV path planning with tangent-plus-Lyapunov vector field guidance and obstacle avoidance, IEEE Trans. Aerosp. Electron. Syst. 49 (2013) 840–856.
[3] P. Corke, S. Hutchinson, A new partitioned approach to image-based visual servo control, IEEE Trans. Robotics Autom. 17 (2001) 507–515.
[4] M. Corless, G. Leitmann, Continuous state feedback guaranteeing uniform ultimate boundedness for uncertain dynamic systems, IEEE Trans. Autom. Control 26 (1981) 1139–1144.
[5] W.E. Dixon, Adaptive regulation of amplitude limited robot manipulators with uncertain kinematics and dynamics, IEEE Trans. Autom. Control 52 (2007) 488–493.
[6] H. Ergezer, K. Leblebicioglu, Path planning for UAVs for maximum information collection, IEEE Trans. Aerosp. Electron. Syst. 49 (2013) 502–520.
[7] O. Faugeras, Three-Dimensional Computer Vision: A Geometric Viewpoint, MIT Press, Cambridge, MA, 1993.
[8] O. Faugeras, F. Lustman, Motion and structure from motion in a piecewise planar environment, Int. J. Pattern Recognit. Artif. Intell. 2 (1988) 485–508.
[9] N.R. Gans, A. Dani, W.E. Dixon, Visual servoing to an arbitrary pose with respect to an object given a single known length, in: Proceedings of the American Control Conference, Seattle, WA, USA, 2008, pp. 1261–1267.
[10] P. Garnell, D.J. East, Guided Weapon Control Systems, Pergamon Press, Oxford, 1977.
[11] S. Kim, H. Oh, A. Tsourdos, Nonlinear model predictive coordinated standoff tracking of a moving ground vehicle, J. Guid. Control Dyn. (2013) 1–10.
[12] E. Malis, F. Chaumette, 2 1/2 D visual servoing with respect to unknown objects through a new estimation scheme of camera displacement, Int. J. Comput. Vis. 37 (2000) 79–97.
[13] V. Malyavej, I.R. Manchester, A.V. Savkin, Precision missile guidance using radar/multiple-video sensor fusion via communication channels with bit-rate constraints, Automatica 42 (2006) 763–769.
[14] I. Manchester, A. Savkin, F. Faruqi, Optical-flow based precision missile guidance inspired by honeybee navigation, in: Proceedings of the 42nd IEEE Conference on Decision and Control, 2003, pp. 5444–5449.
[15] I.R. Manchester, A.V. Savkin, Circular-navigation-guidance law for precision missile/target engagements, J. Guid. Control Dyn. 29 (2006) 314–320.
[16] S. Mehta, W.E. Dixon, D. MacArthur, C.D. Crane, Visual servo control of an unmanned ground vehicle via a moving airborne monocular camera, in: Proceedings of the American Control Conference, Minneapolis, Minnesota, 2006, pp. 5276–5281.
[17] S. Mehta, K. Kaiser, N. Gans, W.E. Dixon, Homography-based coordinate relationships for unmanned air vehicle regulation, in: Proceedings of the AIAA Guidance, Navigation, and Control Conference, Keystone, Colorado, 2006, AIAA 2006-6718.
[18] S.S. Mehta, W. MacKunis, J.W. Curtis, Adaptive vision-based missile guidance in the presence of evasive target maneuvers, in: 18th IFAC World Congress, 2011, pp. 5471–5476.
[19] S.S. Mehta, W. MacKunis, E.L. Pasiliao, J.W. Curtis, Adaptive image-based visual servo control of an uncertain missile airframe, in: Proceedings of the AIAA Guidance, Navigation, and Control Conference, 2005, AIAA 2012-4901.
[20] S. Miwa, F. Imado, T. Kuroda, Clutter effect on the miss distance of a radar homing missile, J. Guid. Control Dyn. 11 (1988) 336–342.
[21] F.W. Nesline, P. Zarchan, Missile guidance design tradeoffs for high-altitude air defense, J. Guid. Control Dyn. 6 (1983) 207–212.

[22] P. Pagilla, B. Yu, An experimental study of planar impact of a robot manipulator, IEEE/ASME Trans. Mechatron. 9 (2004) 123–128.
[23] P.N. Pathirana, A.V. Savkin, Sensor fusion based missile guidance, in: Proceedings of the 6th International Conference on Information Fusion, 2003, pp. 253–260.
[24] V. Shaferman, T. Shima, Unmanned aerial vehicles cooperative tracking of moving ground target in urban environments, J. Guid. Control Dyn. 31 (2008) 1360–1371.
[25] G. Siouris, Missile Guidance and Control Systems, Springer Science & Business Media, New York, 2004.
[26] V. Stepanyan, N. Hovakimyan, Adaptive disturbance rejection controller for visual tracking of a maneuvering target, J. Guid. Control Dyn. 30 (2007) 1090–1106.
[27] T.H. Summers, M.R. Akella, M.J. Mears, Coordinated standoff tracking of moving targets: control laws and information architectures, J. Guid. Control Dyn. 32 (2009) 56–69.
[28] Y. Tian, Y. Li, Z. Ren, Vision-based adaptive guidance law for intercepting a manoeuvring target, IET Control Theory Appl. 5 (2011) 421–428.
[29] B. Uhrmeister, Kalman filters for a missile with radar and/or imaging sensor, J. Guid. Control Dyn. 17 (1994) 1339–1344.
[30] V.A. Vepretsky, Prospects for aerial reconnaissance in combat and operations, Mil. Thought 21 (2012) 107–112.
[31] R. Yanushevsky, Modern Missile Guidance, CRC Press, Boca Raton, 2008.
[32] P. Zarchan, Tactical and Strategic Missile Guidance. Progress in Astronautics and Aeronautics, vol. 176, AIAA, New York, 1998.
[33] E. Zergeroglu, W.E. Dixon, A. Behal, D.M. Dawson, Adaptive set-point control of robotic manipulators with amplitude-limited control inputs, Robotica 18 (2000) 171–181.
[34] Z. Zhang, On the optimization criteria used in two-view motion analysis, IEEE Trans. Pattern Anal. Mach. Intell. 20 (1998) 717–729.
[35] Z. Zhang, A. Hanson, Scaled Euclidean 3D reconstruction based on externally uncalibrated cameras, in: Proceedings of the IEEE International Symposium on Computer Vision, 1995, pp. 37–42.